JOURNAL OF GEOPHYSICAL RESEARCH, VOL. 108, NO. B7, 2347, doi:10.1029/2002JB002073, 2003

# Interplay between tectonics, climate, and fluvial transport during the Cenozoic evolution of the Ebro Basin (NE Iberia)

Daniel Garcia-Castellanos
Faculty of Earth Sciences, Vrije Universiteit, Amsterdam, Netherlands

Jaume Vergés
Institute of Earth Sciences "Jaume Almera," Consejo Superior de Investigaciones Científicas, Barcelona, Spain

Jorge Gaspar-Escribano and Sierd Cloetingh
Faculty of Earth Sciences, Vrije Universiteit, Amsterdam, Netherlands

Received 4 July 2002; revised 5 February 2003; accepted 18 March 2003; published 26 July 2003.

[1] Three-dimensional modeling that integrates fluvial sediment transport, crustal-scale tectonic deformation, and lithospheric flexural subsidence is carried out to simulate the landscape and drainage evolution of the Ebro sedimentary basin (NE Iberia). The Ebro Basin underwent a long period of closed intramountain drainage as a result of tectonic topography generation at the Pyrenees, the Iberian Range, and the Catalan Coastal Range. In the late Oligocene, the Catalan Coastal Range underwent extension leading to the formation of the Valencia Trough (NW Mediterranean), but the Ebro Basin remained closed for nearly 15 Myr more before the Ebro River cut through the remnants of the topographic barrier. This drainage opening caused widespread basin incision that shaped spectacular outcrops of the syntectonic and posttectonic infill. Here we investigate the processes controlling these major drainage changes. The modeling results, constrained by a large data set on the tectonic and transport evolution of the area, predict a closed phase characterized by a large lake in the central eastern Ebro Basin. Dry climatic conditions probably lowered the lake level and contributed, together with rift flank uplift, to prolong this endorheic basin stage. The age and amount of reworked sediment after the opening are consistent with an onset of basin incision between 13 and 8.5 Ma as a result of lake capture by escarpment erosion and lake level rise associated with sediment accumulation and wetter climatic conditions. Sea level changes in the Mediterranean had no major impact in the large-scale drainage evolution of the Ebro Basin. *INDEX TERMS:* 1625 Global Change: Geomorphology and weathering (1824, 1886); 1815 Hydrology: Erosion and sedimentation; 3210 Mathematical Geophysics: Modeling; 3344 Meteorology and Atmospheric Dynamics: Paleoclimatology; 8102 Tectonophysics: Continental contractional orogenic belts; *KEYWORDS:* Pyrenees, drainage evolution, lake, sediment budget, erosion, flexure

**Citation:** Garcia-Castellanos, D., J. Vergés, J. Gaspar-Escribano, and S. Cloetingh, Interplay between tectonics, climate, and fluvial transport during the Cenozoic evolution of the Ebro Basin (NE Iberia), *J. Geophys. Res.*, *108*(B7), 2347, doi:10.1029/2002JB002073, 2003.

## 1. Introduction

[2] Endorheic drainage basins (also called landlocked, internally drained, or closed drainage basins in the literature) are essential in understanding the evolution of sedimentary basins because they do not fit the notion that erosional products from orogens are carried to the oceans. Particularly in intraorogenic cases such as the Altiplano or the Tibetan Plateau, endorheic basins can trap important sediment accumulations at high elevations above sea level [e.g., *Sobel et al.*, 2003]. Endorheic basins occupy 20% of the Earth's land surface but they collect only about 2% of global river runoff, showing that they develop mostly under arid conditions. The Ebro Basin is a well-documented example of a long-lasting intraorogenic endorheic basin, the deposits of which are presently found more than 1000 m above sea level. Because its sedimentary infill has been heavily incised and exposed as a result of a later drainage opening toward the ocean, the Ebro Basin can be regarded as a natural laboratory to study the interplay between tectonics, climate, and sediment transport [e.g., *Arenas et al.*, 2001].

[3] The formation of the Ebro foreland basin began during the Paleocene by flexural subsidence related to the growth of three surrounding Alpine ranges: the Pyrenees to the north (collisional orogenic chain), and the Catalan Coastal Range and Iberian Range to the SE and SW,


0148-0227/03/2002JB002073$09.00

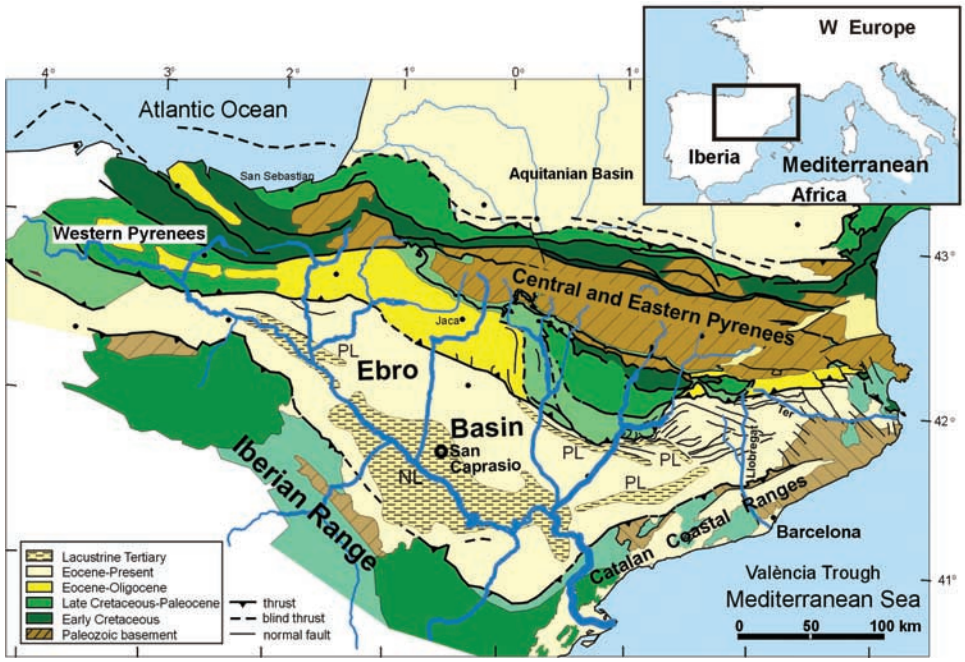


**Figure 1.** Geological map of the Pyrenees, Catalan Coastal Range, and Iberian Range bounding the Ebro Basin. The map shows the present river network and the approximate extent of Neogene lacustrine deposits within the basin (compiled from *Riba* [1983], *Arenas and Pardo* [1999], and *Cabrera and Saez* [1987]) and their age: PL, Paleogene lacustrine deposits; NL, Neogene lacustrine deposits.

respectively (Figure 1). The converging and partially synchronous tectonic shortening along the Pyrenees and the Iberian Range closed the western connection of the basin to the Atlantic Ocean in the earliest late Eocene, starting a long endorheic period of lacustrine deposition that lasted through the Oligocene and most of the Miocene [*Riba et al.*, 1983]. The Ebro foreland basin was syntectonically and posttectonically "backfilled" [*Coney et al.*, 1996] during this period with conglomerates burying most of the frontal tectonic structures of the southern Pyrenees.

[4] At the late Oligocene-early Miocene, the southeastern topographic barrier formed by the Catalan Coastal Range underwent tectonic inversion leading to the extensional reactivation of former reverse faults and ultimately producing rifting along the present Valencia Trough in NW Mediterranean [e.g., *Bartrina et al.*, 1992]. However, the internal drainage of the Ebro Basin did not open to the Mediterranean until late Miocene, and therefore it cannot be linked exclusively to the effect of the extensional tectonics on the relief. The impressive present exposures of the compressive syntectonic Eocene sediments are the result of this drainage opening and the later deep river incision that transported reworked sediments to the Ebro Delta in the Valencia Trough.

[5] The origin of this major drainage change is not well understood. Frequent eustatic sea level changes during Miocene and Pliocene have been suggested as causes of the opening of the largest interior Iberian Basins: Duero, Ebro, and Tajo [*Calvo et al.*, 1993]. In particular, the opening of the Ebro Basin and the development of the present Ebro River have been related [*Riba et al.*, 1983; *Serrat*, 1992] to the sediment overfilling of the lake and the capture (piracy) by one of the Miocene streams draining to the Mediterranean side of the Catalan Coastal Range by the Mediterranean. To date, these proposed mechanisms of opening of the drainage lack a quantitative validation. The Miocene sediments of the delta are poorly imaged by seismic reflection data due to the presence of Messinian salt deposits. Consequently, it has been often assumed that major sedimentation in the Valencia Trough started during the Messinian [e.g., *Nelson and Maldonado*, 1990; *Coney et al.*, 1996]. This led to the hypothesis that the large Messinian sea level drop in the Mediterranean [e.g., *Hsu et al.*, 1972; *Krijgsman et al.*, 1999] may have triggered the capture of the Ebro endorheic drainage by one of the Mediterranean streams [*Coney et al.*, 1996]. However, seismic and borehole data show evidence for enhanced sedimentation rates and deltaic progradations prior to the Messinian [*Dañobeitia et al.*, 1990; *Ziegler*, 1988].

[6] The aim of this paper is to obtain a process-based understanding of the drainage evolution of the Ebro Basin from its closure at upper Eocene times to the present deeply incised situation, readdressing the timing of the drainage opening to the Mediterranean. For this purpose, we compile geophysical, geographical, geological, and paleoclimatic data of the Ebro and Mediterranean Basins and the surrounding cordilleras. These data are integrated in a numerical model [*Garcia-Castellanos*, 2002] that couples fluvial transport, crustal tectonic deformation, and regional isostasy, and that quantitatively links the mass budget between the Ebro Basin and the surrounding mountain ranges to the tectonic evolution of the region.

## 2. Recent Transport in the Ebro Basin

[7] We first use the present topography and recent sediment transport rates to calibrate surface transport parameters

that can be extrapolated to the basin evolution later in this work.

### 2.1. Recent Topography, Drainage, and Sediment Transport Constraints

[8] The present Ebro River is 928 km long and drains a roughly triangular catchment with an area of 85,820 km$^2$ delimited by the Pyrenees, the Iberian Chain, and the Catalan Coastal Range (Figure 1). The relief of the Ebro Basin results from major incision of the Ebro and its tributaries, which excavate the Tertiary sedimentary infill up to 1600 m, as documented in its NE termination [*Lewis et al.*, 2000]. The Ebro River flows out of the Ebro Basin through a succession of gorges that cut through the Catalan Coastal Range. Although the outlet path from the Ebro Basin to the delta is 65 km long, the line distance between the sedimentary basin and the coast is only 32 km, and the minimum width of the Catalan Coastal Range is as little as 8 km in the area.

[9] The 152 present dams in the Ebro catchment have a water storage capacity equivalent to 41.9% of the annual discharge of the basin and modify substantially the natural regime of water and sediment flow. Prior to their construction, the mean water discharge at the Tortosa gauging station (located 47.8 km upstream from the Ebro River mouth) was 1530 m$^3$/s (RivDIS 1.0 database [*Vörösmarty et al.*, 1996]). This represents about 74% of the mean precipitation in the hydrographic basin, with the rest being lost by evapotranspiration. Compilations of runoff distribution [*Korzoun et al.*, 1977] show that most of this evapotranspiration occurs before the water enters the drainage network.

[10] The rate of sediment delivery to the Ebro Delta has been estimated at 316 kg/s during the Pliocene [*Nelson*, 1990; *Serra-Raventós*, 1997] and 196 kg/s during the Holocene [*Nelson*, 1990]. In historical times, the sediment supply was increased by human-induced deforestation starting in Roman times, explaining the high suspended sediment (470–630 kg/s) measured in the first half of the twentieth century. After the extensive dam construction starting in the 1960s, the sediment delivery to the delta strongly decreased to values ranging between 4.7 and 69.7 kg/s. Because the estimations for the Pliocene and Holocene are not affected by human activity, in the following, we use those as a constraint for the parameters controlling the surface transport model.

### 2.2. Surface Transport Model

[11] The surface transport numerical model adopted here assumes that the main agent of basin-scale incision and transport is the fluvial network following the formulation by *Beaumont et al.* [1992] and *Kooi and Beaumont* [1994]. Although there is an ongoing discussion on the optimal empirical relationships governing these processes [e.g., *Willgoose et al.*, 1991; *Howard et al.*, 1994; *Whipple and Tucker*, 1999], this is of secondary importance here, as our analysis focuses on the large-scale, first-order features of the interplay between fluvial transport and lithospheric deformation, rather than on the properties of fluvial transport itself. According to the approach by *Beaumont et al.* [1992], the equilibrium transport capacity $q_{\mathrm{eq}}$ of a river (defined as the amount of mass transported by a river producing no net erosion or sedimentation) is proportional to the mean water discharge $Q_w$ and the slope $S$ along the river profile:

$$q_{\mathrm{eq}}(x,y,t) = K_f\ S(x,y,t) Q_w\ (x,y,t) \tag{1}$$

where $K_f$ is the fluvial transport coefficient, for which we adopt a standard value of 60 kg/m$^3$ [e.g., *Kooi and Beaumont*, 1996; *van der Beek and Braun*, 1999]. For comparison with these works, note that here the sediment load has units of [mass]/[time] and $K_f$ has units of [mass]/[volume]. In general, rivers are out of equilibrium such that the amount of material $dq$ eroded/deposited along a river segment of length $dl$ is proportional to the difference between the actual transported sediment $q$ and $q_{\mathrm{eq}}$ following the relation

$$\frac{dq(x,y,t)}{dl} = \frac{1}{l_f}\left(q(x,y,t) - q_{\mathrm{eq}}(x,y,t)\right), \tag{2}$$

where $l_f$ is the length scale of erosion/deposition. Within these approaches, a river can change from incision to deposition by a reduction in $q_{\mathrm{eq}}$, i.e., by a decrease in discharge and/or slope. As water flows down the river, fluvial transport typically evolves from supply-limited to transport-limited.

[12] The main difference between this and previous models is the explicit treatment of lakes forming in local topographic minima and the water loses by evaporation they imply (Figure 2). When a river reaches a lake or the sea, the transported sediment is distributed in all directions from the river mouth and assuming null transport capacity in equation (2). This implies a deposition rate decreasing exponentially with the distance from the river mouth. This approach overlooks other processes affecting the distribution of deposition in deltas and must be regarded as the simplest possible approach that eventually produces lake/basin overfilling by localizing deposition in the vicinity of the river mouth. Lake overfilling by sediment accumulation, together with erosion at the lake outlet (which decreases the water level of the lake) ensures that lakes behave in the model as transitory or ephemeral phenomena that tend to disappear in absence of tectonic relief generation.

### 2.3. Model Calibration With Recent Transport Rates

[13] The transport model is calibrated by using the present topography relief and precipitation to fit the recent transport rates. The topography displayed in Figure 3 is a combination of the USGS GTOPO30 database onshore and ETOPO5 offshore. The present-day topography shows minimum values below 200 m within the Ebro Basin and maximum values above 3000 m in several peaks in the central Pyrenees (Aneto Peak, 3404 m). Minor modifications at some nodes are necessary to allow drainage along gorges and impede the formation of drainage-dam artifacts related to the discretization of the topography. After these modifications, the calculated drainage network fits the path of the major rivers of the study area.

[14] To avoid dealing with the complexity of the hydrological processes involved in evapotranspiration, the water inputs to the model are formulated in terms of water runoff (part of the rainfall delivered to the drainage network) rather than precipitation. We use the runoff distribution compiled

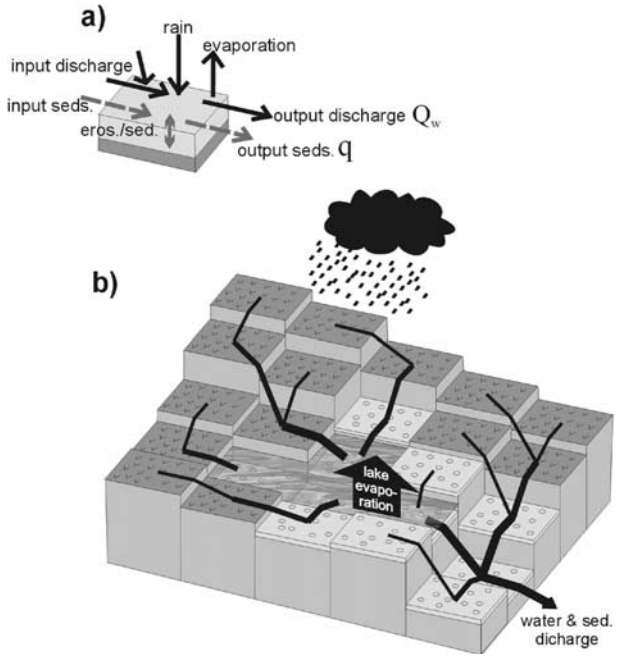


**Figure 2.** Cartoon of the surface processes numerical model. (a) Water and sediment inputs and outputs at each cell of the model. (b) Rivers follow the maximum slope of the discretized topography, taking into account the evaporation at lakes forming in local topographic minima.

by *Korzoun et al.* [1977], which is in good agreement with the historical predam water discharge in the Ebro mouth.

[15] Given these topography and runoff spatial distributions, forward modeling of the recent transport rate to the delta is applied to find the optimum values of the transport parameters. Using the parameters listed in Table 1, the model predicts a sediment load of 240 kg/s, which is in reasonable agreement with the observations described above, ensuring that the obtained set of transport parameters provide a good first approach to the large-scale pattern of erosion and deposition along the catchment of the Ebro River. Although slightly different combinations of parameter values can also fit the sediment load, we choose the one in Table 1 because of its similarity to values used by previous authors [e.g., *Kooi and Beaumont*, 1994]. This parameter set predicts that only 40% of the sediments delivered to the delta comes from the incised Tertiary basin infill rather than the surrounding orogens. We do not have a good control on this ratio because it strongly depends on the contrast of erodability ($l_f$) between the basin and the orogen and because our transport model does not incorporate landsliding or hillslope transport and therefore underestimates the sediment supply in the highlands.

[16] Figure 3 shows the predicted distribution of erosion and sedimentation rate and the isostatic vertical movements related to that surface mass redistribution. The rebound/subsidence distribution follows the long-wavelength trends of the erosion/sedimentation rate distribution, showing localized deposition and subsidence (up to 0.4 mm/yr) in the Ebro Delta and broad-scale erosion and rock uplift (up to 0.15 mm/yr) in the Pyrenees, in agreement with erosion rates estimated from crustal-scale cross sections in the eastern Pyrenees [*Vergés et al.*, 1995] and apatite fission track thermochronology [*Fitzgerald et al.*, 1999]. A remarkable outcome of this calibration is that the sediment load carried to the Mediterranean is sensitive to the isostatic movements: an identical experiment was run without any isostatic compensation (no lithospheric vertical movements), producing a 10% lower sediment delivery at the river mouth. This shows that, even in absence of tectonism, the lithospheric isostatic response exerts a detectable effect on river mass transport.

## 3. Quantitative Constraints on the Ebro Basin Evolution

### 3.1. Tectonic Evolution of the Surrounding Mountain Ranges

[17] The Tertiary evolution of NE Spain is marked by two major events: the continental collision between Iberia and the European plate since Late Cretaceous and the opening of

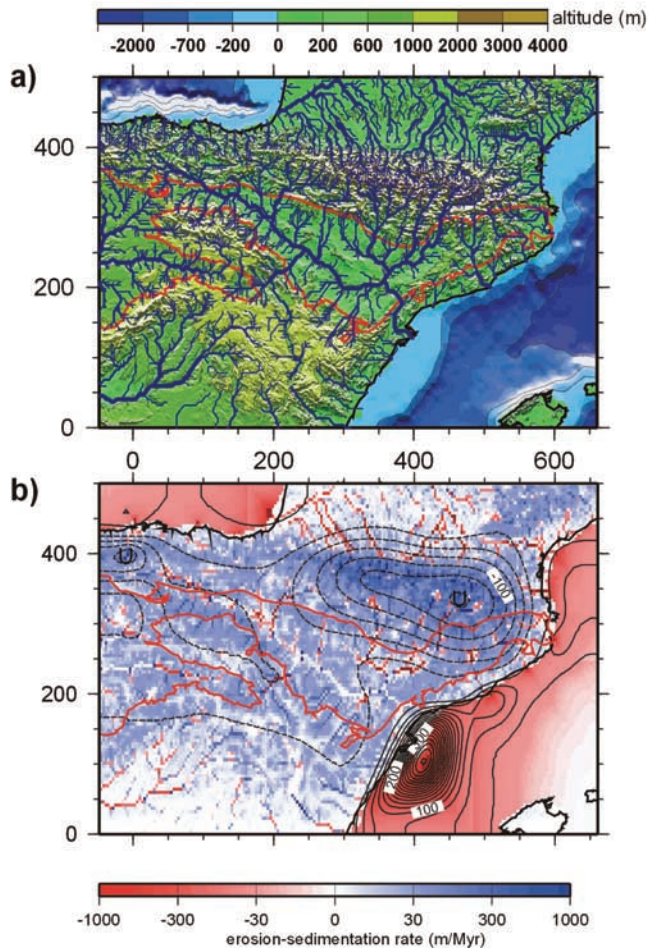


**Figure 3.** (a) Present observed topography and predicted drainage network using the historical mean runoff distribution. River width is proportional to water discharge. (b) Predicted erosion rate (shading) and isostatic vertical velocity of the lithosphere related to the surface transport of mass (isolines every 25 m/Myr). Note that deposition is depicted as negative values. The red line indicates the limit of the Tertiary sedimentary basins with weaker lithology than the surrounding mountain ranges.

**Table 1.** Parameters Used and Derived in the Calibration

| Parameters | Values |
|---|---|
| Runoff (precipitation) distribution | 200 + 300 × altitude [km] mm/yr[1] |
| Gridding | 104 × 55 |
| Lithospheric elastic thickness | 5–25 km |
| Transport coefficient $K_f$ | 60 kg/m$^3$ |
| Length-scale erosion $l_f$ | |
| Basement | 120 km |
| Sediments | 60 km |
| Length-scale deposition $l_f$ | 50 km |
| Density of asthenosphere | 3250 kg/m$^3$ |
| Density of basement and thrusts | 2800 kg/m$^3$ |
| Density of sediment | 2200 kg/m$^3$ |
| Mean porosity sediment | 0.3 |

the Valencia Trough related to the formation of the western Mediterranean. The end of the Pyrenean shortening overlapped with the beginning of the Mediterranean extension during the late Oligocene [e.g., *Roca et al.*, 1999; *Vergés and Sàbat*, 1999].

[18] The continental collision of Iberia and Europe produced the formation of the Pyrenean orogen with a partial subduction of the Iberian lithosphere toward the north [e.g., *Choukroune et al.*, 1989; *Muñoz*, 1992]. The Ebro foreland basin (NE Spain) started its development during early Paleocene synchronous with crustal shortening in the Pyrenees. It remained underfilled and marine until 35 Ma [deposition of Cardona evaporitic level; *Taberner et al.*, 1999] and then became overfilled and continental at the time that the shortening rates along the Pyrenees decreased from 4.5 to 2 mm/yr [*Puigdefàbregas et al.*, 1992; *Vergés et al.*, 1995]. The uplift of the western Pyrenees closed the western connection of the basin with the Atlantic Ocean originating an intramountain basin [*Riba et al.*, 1983; *Burbank et al.*, 1992] limited by the Pyrenees (N), the Catalan Coastal Range (SE), and the Iberian Range (SW). The frontal parts of these mountain ranges were buried by sediments during this stage.

[19] Magnetostratigraphic studies on growth strata at the front of the Pyrenean fold-and-thrust belt show that the end of deformation occurred during upper Oligocene times (~24.7 Ma) [*Meigs et al.*, 1996] and fission track analysis shows that major basement exhumation ended at about 30 Ma with an abrupt decrease by a factor 4–5 of the erosion rates [*Fitzgerald et al.*, 1999].

[20] During the earliest Oligocene, extension in the western Mediterranean started in the Gulf of Lion and propagated toward the SW into the Valencia Trough at the latest Oligocene [*Mauffret et al.*, 1995; *Roca et al.*, 1999] cutting the ancestral Catalan Coastal Range and developing a wide lowland area that was subsequently occupied by the sea [*Roca et al.*, 1999; *Vergés and Sàbat*, 1999]. This extensional episode produced a flexural uplift of the SE margin of the Ebro Basin [*Watts and Torné*, 1992b; *Janssen et al.*, 1993; *Gaspar-Escribano et al.*, 2001] that was reinforced by lateral heat flow from the basin toward the continent at subcrustal levels [*Negredo et al.*, 1999]. This uplift of the footwall of the SE dipping normal fault system preceded the opening of the Ebro fluvial network.

### 3.2. Drainage and Climatic Evolution

[21] The drainage evolution of the Ebro Basin is clearly influenced by its tectonic evolution. The first lacustrine salt deposits are dated as 35 Myr old [*Taberner et al.*, 1999]. After the connection of the Ebro Basin with the Atlantic Ocean was interrupted, a landlocked fluvial network [*Arenas et al.*, 1997] delivered sediments to a basin characterized by a large, shallow lacustrine system [e.g., *Anadón et al.*, 1989; *Arenas and Pardo*, 1999]. The present-day discontinuity of the lacustrine sediment outcrops obscures whether the lacustrine system consisted of a single large lake or a number of smaller lakes, although the first interpretation has been suggested by *Arenas and Pardo* [1999] based on sediment facies observations and paleogeographic reconstructions. It is worth noting that the present-day evaporation rates of 800 mm/yr [e.g., *Colomer et al.*, 1996] would require an evaporation surface larger than 60,000 km$^2$ (nearly 70% of the present area of the Ebro River catchment) to evaporate the present water discharge at the Ebro mouth.

[22] During the latest Oligocene and the Miocene, the Catalan Coastal Range underwent extensional inversion and rifting along the Valencia Trough [*Roca*, 2001]. The upstream erosion of two newly developed Mediterranean rivers (Ter and Llobregat, Figure 1) progressively captured the internal fluvial network in the region located NE of the Ebro Basin [*Lewis et al.*, 2000].

[23] The youngest conglomeratic deposits in the Ebro Basin have been dated as late Miocene in the western edge of the basin [*Muñoz-Jiménez and Casas-Sainz*, 1997], but these deposits do not necessarily imply a high, coeval base level. The most recent lacustrine sediments are in the southern margin of the basin and have been dated as Tortonian based on vertebrate fauna [*Pérez et al.*, 1988, 1994], whereas the uppermost preserved sediments in the center of the basin are 13.5 Ma [*Pérez-Rivarés et al.*, 2002] in age. These dates provide a first approximation of the time at which the endorheic lacustrine system of the Ebro Basin opened to the Mediterranean starting massive basin incision.

[24] The knowledge of the Tertiary climate evolution in the area is only qualitative, which complicates the identification of links with the drainage evolution. A simplified history of the Cenozoic climatic evolution of the Ebro basin can be synthesized from floral and faunal data (Figure 4). Palynological studies show that climate evolved progressively from warm and humid with rich, diverse vegetation at Bartonian (41.3–37 Ma) [*López-Blanco et al.*, 2000] to warm and arid during early Oligocene (33.7–28.5 Ma) [*Cavagnetto and Anadón*, 1996] coinciding approximately with the beginning of the endorheic period. Mammal assemblages show that climate became seasonal and humid during late Miocene with a relative peak at 9.4 Ma [*Alonso-Zarza and Calvo*, 2000; *Calvo et al.*, 1993]. This late Miocene transition from dry to humid climate is also in agreement with macroflora studies carried out by *Sanz de Siria Catalan* [1993]. The concurrence in time of the drainage opening of the basin and this long-term climate transition suggests that the increase in precipitation may be responsible for a lake level rise, eventually triggering the opening of the closed lake. We address this hypothesis with the numerical models developed later in this paper.

### 3.3. Sediment Budget

[25] Three estimates are used to constrain the large-scale mass balance in the orogen/basin system [e.g., *Kuhlemann et al.*, 2001]: the present volume of sediments contained in the

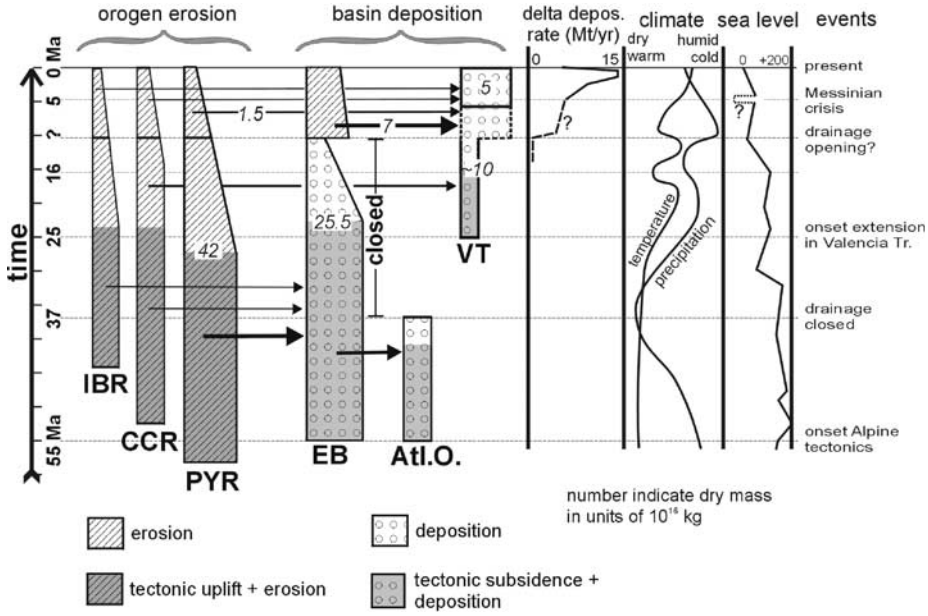


**Figure 4.** Sediment flow diagram between the mountain ranges (IBR, Iberian Range; CCR, Catalan Coastal Range; PYR, southern side of the Pyrenees) and the basins in NE Spain (EB, Ebro Basin; Atl.O, Atlantic Ocean; VT, Valencia Trough). Numbers in italic indicate eroded, transported, and deposited mass of dry sediment in units of $10^{16}$ kg. The post-Messinian mass delivered to the Ebro Delta is smaller than the estimated erosion in the Ebro Basin and the surrounding mountain ranges, indicating that the drainage opening must have occurred before Messinian. Rates of deposition in the Ebro Delta are based on the work of *Nelson* [1990] and *Dañobeitia et al.* [1990]. Climate changes are based on published flora and fauna studies [*Cavagnetto and Anadón*, 1996; *Alonso-Zarza and Calvo*, 2000; *Sanz de Siria Catalan*, 1993]. Long-term sea level changes are simplified after *Haq et al.* [1987].

Ebro Basin, the amount of basin sediments reworked since the opening of the basin to the Mediterranean, and the amount of Neogene sediments accumulated in the Valencia Trough.

[26] To estimate the present volume of clastics within the basin, a map of the thickness of Cenozoic detrital sediment has been constructed (Figure 5) by compilation of seismic and well data [*Lanaja et al.*, 1987], cross sections [*Guimerà and Álvaro*, 1990; *Cámara and Klimowitz*, 1985; *Clavell et al.*, 1988; *Jurado and Riba*, 1996; *Teixell*, 1996; *Turner*, 1996; *Vergés et al.*, 1998; *Sánchez et al.*, 1999; *Salas et al.*, 2001], and previous compilations for La Rioja [*Muñoz-Jiménez and Casas-Sainz*, 1997] and the Valencia Trough [*Watts and Torné*, 1992a; *Torné et al.*, 1996]. This isopach map includes both the undeformed sediments and those deformed by the frontal surrounding thrusts (e.g., in the westernmost part of the basin, in La Rioja) and intermediate piggyback basins of the Pyrenean flank (Miranda, Jaca, Tremp, Ager, and Ripoll). Marine platform limestone and marine salt units have been excluded from this map.

[27] Within the Ebro Basin, the sediment thickness increases toward the north reaching maximum values above 5000 m, and then decreases to zero beneath the Pyrenees, in the footwall cutoff of the Pyrenean thrust system. The present volume of Cenozoic sediments in the Ebro Basin resulting from the integration of the distribution in Figure 5 is 110,000 km$^3$, with an estimated error of ~5000 km$^3$. Using a mean grain density of 2600 kg/m$^3$ and a mean porosity of 0.3 [*Vergés et al.*, 1998], the present mass of clastic sediment in the Ebro Basin results in $20.0 \times 10^{16}$ kg. In the area of the Valencia Trough shown in Figure 5, the volume of Neogene sediments is 92,000 km$^3$ ($17.4 \times 10^{16}$ kg of dry sediment density of 2200 kg/m$^3$ with a mean porosity of 0.3), with maximum thickness >2–4 km along a SW-NE elongated area centered in front of the Ebro mouth. The volume of erosion in the southern flank of the Pyrenees can be estimated by interpolating values derived from restored and balanced sections across the chain [*Roure et al.*, 1989; *Vergés et al.*, 1995; *Muñoz*, 1992; *Teixell*, 1998] and from thermochronology [*Fitzgerald et al.*, 1999], resulting in 157,000 km$^3$ ($42 \times 10^{16}$ kg assuming a density of 2800 kg/m$^3$), with an uncertainty of >30%. *Nelson* [1990] estimated the post-Messinian sediment delivery of the Ebro River to the delta and the Valencia Trough to be 27,000 km$^3$, equivalent to $4.8 \times 10^{16}$ kg of dry clastic sediment.

[28] To complete the sediment budget summarized in Figure 4, a minimum estimation of the amount of sediments eroded after the opening is calculated by subtracting the present topography of the basin from the reconstructed paleotopography of the basin at its maximum infill (at Tortonian times). The present remains of lacustrine sediments are found at altitudes above 800 m (e.g., at San Caprasio, Figure 1). Conglomerates brought from the Pyrenees to the margin of the basin are presently found at elevations higher than 1500 m, and *Coney et al.* [1996] suggested that the frontal structures of the Pyrenees were buried by 2–3 km of sediment. A mean slope of 1° toward the center of the basin would imply 870 m of topographic difference between the center and the margins. Thus a low estimation of the mean altitude of the basin sediments at the opening time would be $H_s$ = 1000 m, which results in

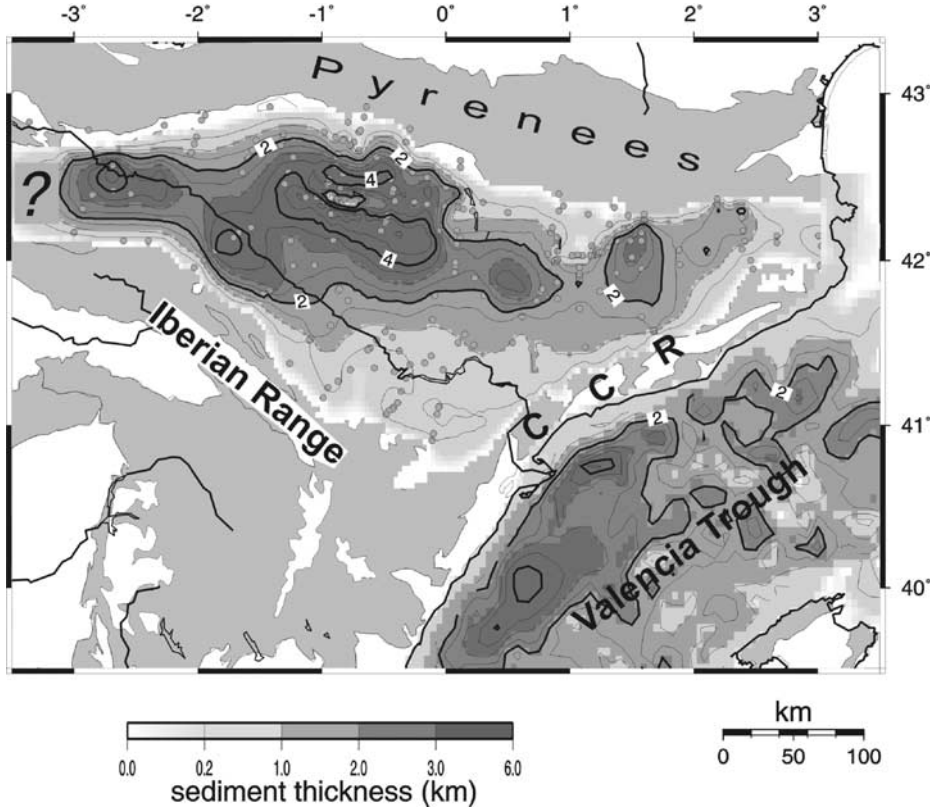


**Figure 5.** Present thickness of Tertiary sediments of the Ebro Basin (this work) and Neogene sediments in the Valencia Trough (compiled by *Watts and Torné* [1992a]).

30,100 km$^3$ of erosion, whereas for $H_s$ = 1200 m the missing volume would be 45,400 km$^3$. In addition to these denuded sediments, erosion products of the surrounding ranges were also delivered to the delta. Assuming a constant postcompression denudation rate 5 times smaller than during the synshortening phase [*Fitzgerald et al.*, 1999], this represents at least 10,000 km$^3$ of additional sediment. Thus the total sediment transported to the delta after the opening of the Ebro Basin ranges between 40,100 and 55,400 km$^3$ ($6.3 \times 10^{16}$–$8.6 \times 10^{16}$ kg of dry sediment with a density of 2200 kg/m$^3$ and a porosity of 0.3).

[29] Though we must keep in mind the uncertainties inherent to these calculations, it seems that the post-Messinian delta estimated by *Nelson* [1990] in $4.8 \times 10^{16}$ kg does not account for the complete postopening incision of the Ebro Basin. If the post-Messinian deposition rates are extrapolated to the whole incision period, the opening of the basin should have occurred between 8.5 and 12 Ma. This issue is addressed below by means of numerical modeling of the basin evolution and comparison to independent studies.

## 4. Modeling the Ebro Basin Evolution

[30] In order to better understand the drainage evolution of the Ebro Basin, we apply a numerical model integrating the described surface transport model with quantitative approaches to the tectonic processes of thrusting and isostasy.

### 4.1. Numerical Model

[31] Quantitative studies of the interplay between lithosphere dynamics and drainage networks in sedimentary basins are scarce. Since the early models of foreland basin formation in the 1980s, the lithospheric flexural response to orogenic thrust stacking has been accepted as the key process generating accommodation space and localizing sediment accumulation next to orogens [e.g., *Beaumont*, 1981; *Flemings and Jordan*, 1989; *Sinclair and Allen*, 1992; *Ford et al.*, 1999; *Garcia-Castellanos et al.*, 2002]. However, these studies used simplistic approaches for the surface transport of mass, neglecting the dynamics and three dimensionality of fluvial networks. Later numerical experiments showed that the spatial and temporal distribution of sediment facies is strongly influenced by the 3D character of fluvial transport [*Johnson and Beaumont*, 1995], and that the coupled tectonic-fluvial network system may control the evolution of sediment delivery from orogens [*Tucker and Slingerland*, 1996]. In turn, drainage networks in the foreland basin can be under certain conditions controlled by the flexural behavior of the lithosphere [*Burbank*, 1992; *Garcia-Castellanos*, 2002].

[32] The numerical model applied here to study the drainage and sedimentary basin evolution is based on the approach developed by *Garcia-Castellanos* [2002] and incorporates planform numerical solutions to the following processes (Figures 6 and 7): (1) tectonic deformation is mainly driven by upper crustal thrust stacking and normal faulting; (2) surface transport is driven by the fluvial network as previously described; and (3) the mass redistribution resulting from (1) and (2) is compensated by regional isostasy (lithospheric flexure).

[33] Tectonic deformation is simulated with units (or blocks) moving relative to the foreland. These units pre-

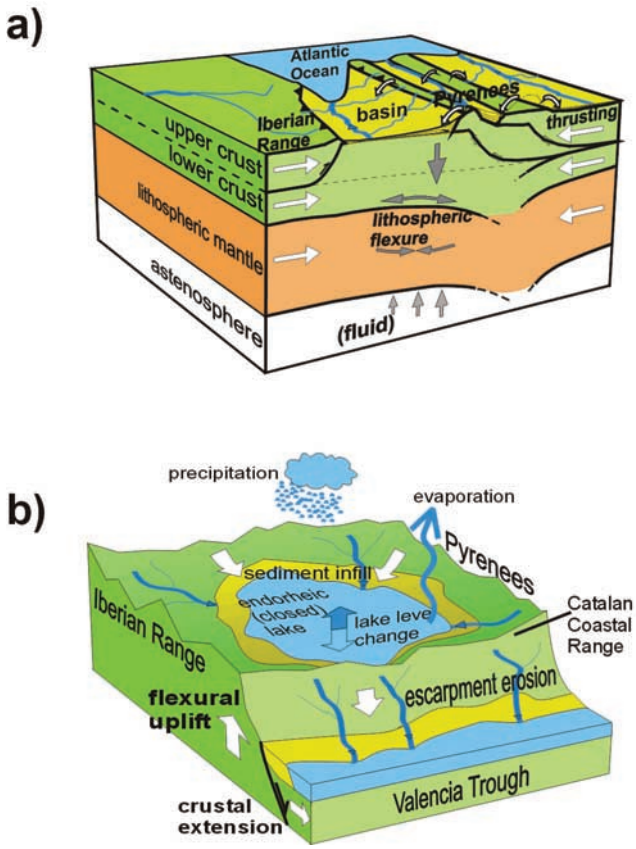


**Figure 6.** (a) Cartoon of the conceptual model of formation of the early Ebro foreland basin. Closure of the drainage occurred due to superposition of tectonic shortening along the Iberian Range and the Pyrenees. White arrows indicate surface and tectonic transport. (b) Endorheic stage: processes involved in the later drainage opening by capture of the closed lake that have been incorporated in the numerical model.

serve their vertical thickness during movement (vertical shear approach) simulating a noninstantaneous tectonic deformation. It is not the intention of our modeling to reproduce either the internal geometry of the orogenic wedge or the details of the kinematics of its evolution [*Beaumont et al.*, 2000]. For this reason, and for the sake of simplicity, crustal shortening in each mountain range is represented in the model by the minimum number of block units necessary (1 and 2 in the model described later) and a constant shortening rate.

[34] Isostatic subsidence and uplift are calculated assuming that the lithosphere behaves as a 2D thin elastic plate [e.g., *van Wees and Cloetingh*, 1994] lying on a fluid asthenosphere and loaded by the large-scale mass redistribution.

[35] Erosion and sedimentation is calculated as described in section 2.2 by defining the drainage network on top of the time-dependent topography resulting from tectonic deformation and isostasy. To account for the endorheic stage of the Ebro Basin, lake evaporation has been incorporated in the model as an improvement on the algorithm by *Garcia-Castellanos* [2002]. The amount of lake evaporation is calculated by multiplying the lake surface by a constant evaporation rate and subtracting the result to the lake output discharge. Evaporation can eventually eliminate the excess of water in the lake and reduce its level below the outlet causing closure of the basin.

[36] As a result of the coupled response of these processes, the numerical model provides the 3D evolution of the geometry of the orogen/basin system, including topography, drainage networks, sediment horizons, erosion distribution, and vertical isostatic movements.

### 4.2. Parameterization of Lake Capture

[37] A synthetic model of lake capture or piracy has been designed to evaluate the importance of the parameters involved in a large-scale drainage change such as that which took place in the Ebro Basin (Figure 8). No tectonic deformation is considered in this model, in which all vertical movements are related to the isostatic compensation of the surface mass transport. As a proxy for the situation of the Ebro Basin and surrounding ranges at the end of the major tectonism, the initial topography corresponds to a rectangular drainage basin with a height of 1400 m in its perimeter and 800 m at the center. In the eastern side of this model there is a 1000 m deep sea separated from the western basin by an N-S oriented escarpment that is 1400 m high.

[38] Based on the parameter values derived in the calibration (Table 1), water loses from the drainage network are controlled by lake evaporation. We use a value of 1300 mm/yr and a precipitation of 400 mm/yr. Because the total runoff collected in the model lake (420 $m^3/s$) is one third of the potential evaporation in the whole catchment, the area of the closed lake results in one third of the catchment, to be in hydrological equilibrium between water inputs and evaporation. From an initial ($t$ = 0) altitude at 953 m (see initial stage in Figure 8), the modeled lake level increases by accumulation of sediment. At $t$ = 21 Myr, the level of the lake equals the minimum altitude at the eastern divide (this outlet is at 1040 m), producing the opening of the drainage (Figure 8).

[39] A first-order parameter determining the time of capture is the width of the initial barrier. The initial topography used in this parameterization implies a distance

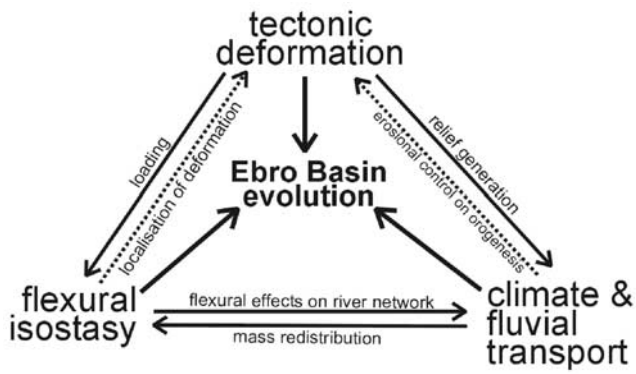


**Figure 7.** Conceptual cartoon illustrating processes involved in controlling drainage evolution and large-scale sediment transport in the Ebro Basin and surrounding mountain ranges. Solid arrows indicate the interactions addressed in the present work; dotted arrows indicate interactions not explicitly considered in the models here.

from the lakeshore to the sea of 15 km at $t = 0$ Myr, similar to the distance between the Ebro lacustrine sediments and the eastern flank of the Catalan Coastal Range, nearby the outlet of the Ebro [e.g., *Cabrera et al.*, 2002]. A higher evaporation rate would predict a lower lake level and thus a longer distance from the lake to the coast. The precipitation and the evaporation rates are also main parameters controlling the lake level and the time of capture. Humid conditions (high precipitation and/or low evaporation) speed up the process by raising the lake level and the erosion in the escarpment.

[40] Isostasy delays the time of capture because it uplifts the eroded topographic barrier. Repeating this model for different values of lithospheric elastic thickness ($T_e$) leads to the opening time distribution displayed in Figure 8b. Local isostasy ($T_e = 0$) predicts a slower capture at $t = 28$ Myr, whereas higher $T_e$ values reduce the isostatic vertical movements and accelerate the drainage opening ($t = 11$ Myr for $T_e = \text{inf.}$).

[41] The time required for the capture of the whole lake is 0.8 Myr, measured from the first contact of the capturing stream with the lake until the lake extension reduces to zero. However, the time in which the capture becomes irreversible is significantly shorter: In only 0.2 Myr the outlet altitude decreases by 212 m. In order to close the drainage again a similar drop in the lake level would be required. Such a lake level drop would imply an abrupt and long-lasting reduction by a factor 5 in precipitation or an equivalent increase in evaporation, for which there is no reported evidence in the Ebro Basin. The time lag required for capture, however, must be regarded as indicative because it is sensitive to the resolution of the model.

[42] The same parameterization is undertaken using twice the rate of precipitation (dashed line in Figure 8b), causing a faster capture of the lake as a result of higher sediment delivery and escarpment erosion and because the equilibrium level of the lake becomes higher. Introducing a decrease of 500 m of the sea level during 1 Myr between $t = 10$ Myr and $t = 11$ Myr has little effect in accelerating the time of capture (Figure 8b). These results suggest that the flexural isostatic compensation and the climate changes exert far more control on the time lapse required for lake capture than base level changes in the adjacent sea.

### 4.3. Setup of the Ebro Evolution Model

[43] In order to reproduce the closure and opening of the Ebro Basin, our evolutionary model of the Ebro Basin incorporates a simplification of the history of tectonic deformation described above. The model spans from $t = 60$ Ma to $t = 0$ Ma (present). The adopted initial topography (representing the pre-Tertiary situation) is slightly above the coeval sea level throughout most of the modeled region and exerts little influence in the model results. An exception is the 900 m pre-Tertiary relief in the SW of the model (in the present-day location of the Iberian Range), which is necessary to maintain the centripetal drainage. Sea level changes have been adopted from *Haq et al.* [1987] to further strengthen the preceding result that base level variations in the Mediterranean had little effect on escarpment erosion on the time and spatial scales of our study. We maximize the base level drop effect of the Mediterranean desiccation during the Messinian [e.g., *Aharon et al.*, 1993] by lowering the sea level 500 m between 6.14 and 5.26 Ma, although recent studies show that the desiccation was probably deeper but about 10 times shorter [*Krijgsman et al.*, 1999].

[44] The kinematics adopted for the tectonic deformation is shown in Figure 9 and Table 2. Based on the detachment levels obtained from geological reconstructions [e.g., *Muñoz-Jiménez and Casas-Sainz*, 1997; *Muñoz*, 1992; *Roca and Guimerà*, 1992], each tectonic unit is defined by a fault that becomes horizontal at 11 km depth and moves with a constant velocity relative to the pre-Tertiary basement, which is taken as the *x*-*y* reference frame. Shortening is active from the beginning of the model until 28 Ma along the two northern E-W striking faults (Pyrenees); from 55 to 26 Ma in the Catalan Coastal Range and from 38 to 26 Ma in the Iberian Chain. The opening of the Valencia Trough is active from 23.5 to 8 Ma. The total shift of these units is 80 km for the Pyrenees (southward), 14 km for the Catalan Coastal Range (northward), and 33 km for the Iberian Range (northward). Extension in the Mediterranean amounts to 197 km southeastward. These kinematics fit satisfactorily the magnitude of shortening derived from restored geological cross sections of the Pyrenees [*Vergés et al.*, 1995]. Shortening along the Catalan Coastal Range is usually considered to be smaller, on the order of 8 km [e.g., *Lawton et al.*, 1999]. However, these estimates account only for the perpendicular component of shortening on the frontal thrust and overlooks shortening along other faults that have been overprinted by the Neogene extension. The 14-km shortening adopted for our modeling is required to reproduce the closure of the basin and the paleotopography inferred by *López-Blanco et al.* [2000]. As for the Iberian Range, *Muñoz-Jiménez and Casas-Sainz* [1997], based on industry seismic data, report a minimum northward displacement of 25 km. *Salas et al.* [2001] calculated a total Paleogene shortening across the Iberia Range of 55–75 km. This is a maximum estimation for our model because it also includes south verging shortening at the southern side of the range. Furthermore, part of that shortening predates the initial time of the model explaining the initial topography of 1000 m adopted at the southwestern part of the model.

[45] For the flexural calculations, we adopt the elastic thickness obtained by *Gaspar-Escribano et al.* [2001] for the Ebro Basin, showing relative low lithospheric rigidity similar to other Alpine foreland basins. At the Valencia Trough, *Watts and Torné* [1992b] and *Janssen et al.* [1993] obtained low rigidities consistently with the high heat flow and lithospheric thinning in this domain [*Negredo et al.*, 1999] and suggesting an almost local isostasy situation. Following these authors, we use an overall equivalent elastic thickness of 25 km that is reduced to 5 km across the Catalan Coastal Range and at the westernmost corner of the basin.

[46] As for the surface transport, rain, evaporation, and transport parameters are assumed constant throughout the basin evolution. The present-day runoff distribution [*Korzoun et al.*, 1977] shows regional variations dependent mainly on altitude and latitude. Rather than applying the present runoff distribution to the whole basin evolution, we find a simple linear expression of runoff as a function of altitude and latitude:

$$\text{runoff}(\text{mm/a}) = (R + K_R\, h)(1 + d/L_R), \qquad (3)$$

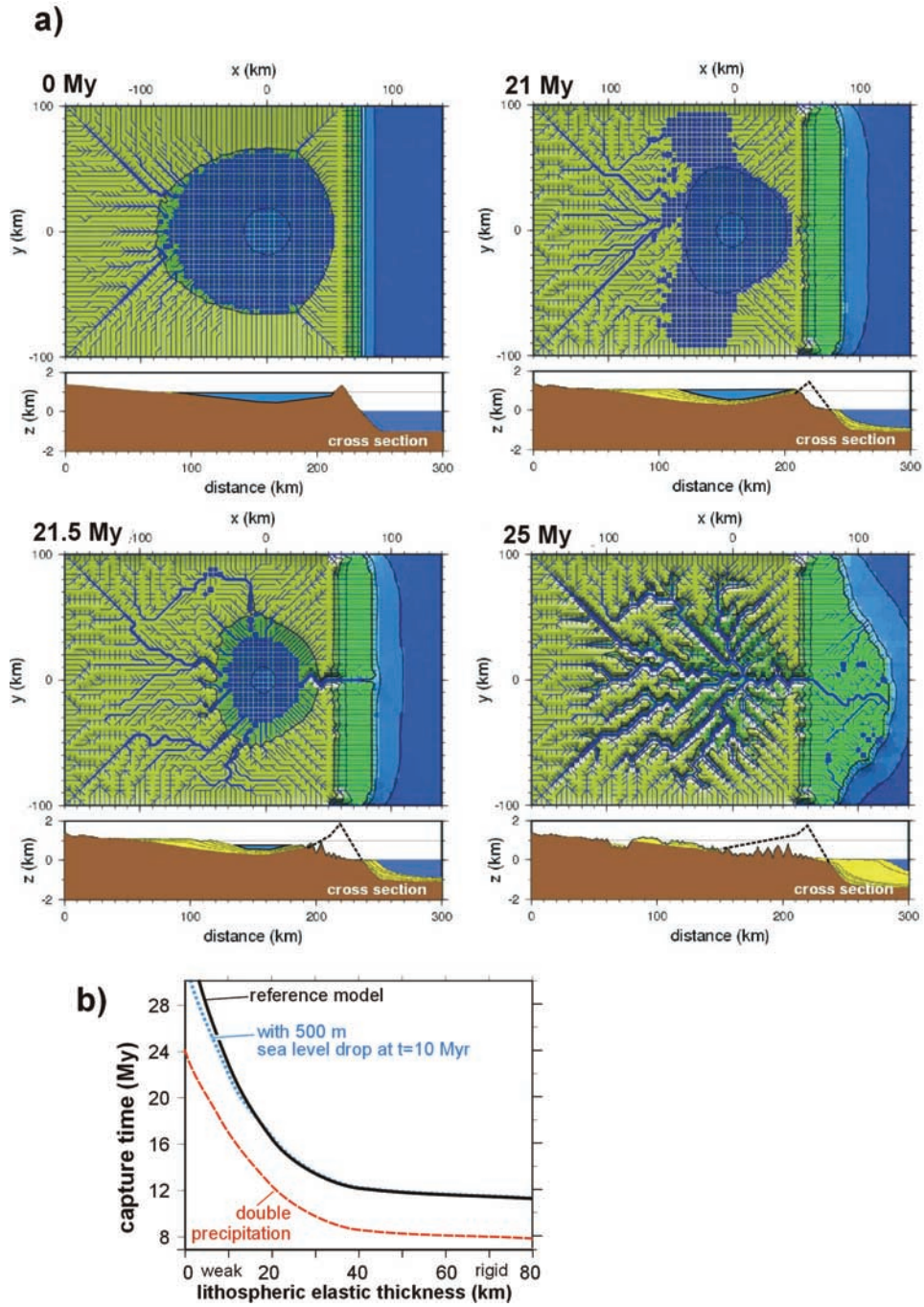


**Figure 8.** Evolution of a synthetic numerical model of lake capture. (a) Topography, drainage network, and cross section of the model along $y = 0$ are shown at four stages. Rivers are drawn with line width proportional to their predicted water discharge. Capture of the endorheic basin occurs between 21 and 21.5 Myr. (b) Time lapse required for lake capture as a function of flexural elastic thickness, precipitation, and sea level changes.

where $h$ is the elevation in kilometers and $d$ is the distance to the central latitude of the model ($y = 250$ km). The runoff at sea level $R$ and the constants of proportionality to altitude ($K_R$) and latitude ($L_R$) are determined from the present runoff distribution and the historical (predam) mean water discharge in the Ebro mouth of 1530 $m^3/s$ (Table 1). This expression allows extrapolating the orographic effect on precipitation to the entire model evolution, under the assumption that $R$, $K_R$, and $L_R$ remain constant through time.

### 4.4. Evolution Model Results

[47] Several hundreds of model runs have been tested introducing small differences in each parameter. The results shown in Figures 10–13 correspond to one of the models providing a good fit to the drainage evolution, the paleo-

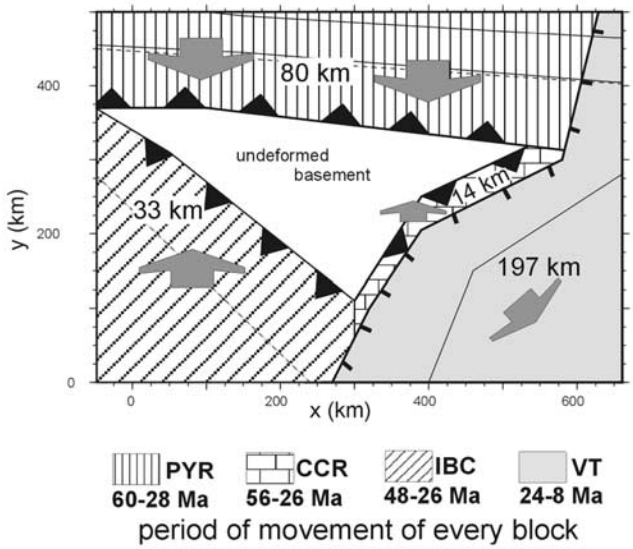


**Figure 9.** Kinematics of shortening (thrusting) and extension used for the model. Numbers in the map indicate the total translation of the upper blocks. Arrows indicate the direction of the upper block movement, relative to the undeformed basement of the basin.

geography, and the sediment budget, with special emphasis on the endorheic (closed) and exorheic (open) phases. The evolution of a cross section shown in Figure 11 exemplifies the 3D geometrical configuration of the moving blocks, the undeformed basement, and the sediments.

[48] The southward displacement of the northern thrusting units (representing the Pyrenees) is the main generator of topography and is responsible for the flexural subsidence along the southern margin of this unit, generating a lineal underfilled foreland basin connected with the boundaries of the model. These marine connections are irreversibly closed at 38 Ma because of the superposition of rock uplift produced along the thrusts accommodating the N-S convergence. Due to the assumption of constant shortening rates, this particular model run does not reproduce the earlier isolation from the sea in the east than in the west. Because this is not relevant for the aims of this paper, we modified the tectonic parameters (fault depth and shortening rates) to fit the later evolution of the basin rather than adding unnecessary complexity to the model.

[49] As the deposited sediments in the basin thicken, their deformation in the frontal part of the Pyrenean units produce a topographic barrier of increasing altitude, eventually producing deflections of the main rivers. Such interaction between drainage networks and tectonic deformation in the External Sierras during middle Eocene to early Miocene times has been reported by *Burbank and Vergés* [1994] and *Arenas et al.* [2001].

[50] From 38 to 26 Ma, the drainage predicted in the model is predominantly endorheic with some periods of exorheic drainage (open toward the east). Periods of lake deposition, however, dominate over shorter periods of river transport (Figure 10). The use of lower evaporation rates and/or higher precipitation rates in other model runs caused the lake to permanently overflow toward the east, defeating the topography generation in the east and inhibiting the landlocked drainage episode. At the end of this period, the maximum altitude of the topographic barrier (representing the Catalan Coastal Range in the model) varies between 700 and 1100 m and its width is about 40 km, within the range of values proposed by *López-Blanco et al.* [2000] based on the study of the alluvial fans deposited in the SE margin of the Ebro Basin.

[51] The model predicts that a centripetal drainage pattern drains toward a single closed lake located in the central eastern side of the basin. The smaller sediment supply from the remnants of the eastern range (representing the Catalan Coastal Range) relative to the other boundaries of the basin provokes the migration of the lake shore toward the east, reducing the distance between the lake and the sea to only 30 km at 23 Ma.

[52] The extensional fault introduced in the model at 23.5 Ma does not reach the domain of the closed basin and thus it does not open the endorheic drainage. Indeed, the remains of the topographic barrier separating lake from sea are uplifted during the extension due to flexural unloading (flank uplift), enhancing substantially the altitude of the barrier. The maximum flank uplift is close to 1000 m. Adding the former Paleogene tectonic uplift (up to 1600 m in the model), the total rock uplift along this range is 2600 m, most of which is consumed by erosion (up to 2000 m).

[53] The altitude of the lake level with respect to the present sea level (Figure 12a) varies significantly during its early stages due to the changes induced by the ongoing tectonic deformation on the drainage. The level of the main lake is sometimes below sea level, indicating that it is endorheic with a low evaporation/precipitation ratio (as presently occurs in the Dead Sea and the Caspian Sea). The experiment indicates that alternation between open and closed drainage was probable in the early lacustrine stages, but not later when the lake became significantly higher. By this stage, the high topographic gradient relative to the Mediterranean Sea would make any short drainage opening to the sea irreversible.

**Table 2.** Parameters of the Evolution Model Corresponding to Figures 10–13

| Parameters | Values |
|---|---|
| Timing | 60–0 Ma |
| Time step | 0.05 Myr |
| Pyrenean kinematics | |
| Timing | 60–28 Ma |
| Velocity | 2.5 S km/Myr |
| Total shortening | 80 km |
| CCR kinematics | |
| Timing | 56–26 Ma |
| Velocity | 0.47 N km/Myr |
| Total shortening | 14 km |
| Iberian kinematics | |
| Timing | 48–26 Ma |
| Velocity | 1.5 N km/Myr |
| Total shortening | 33 km |
| Valencia Trough kinematics | |
| Timing | 23.5–8 Ma |
| Velocity | 9°S, 9°E km/Myr |
| Total extension | 197 km |
| Runoff (precipitation) | $(100 + 200 \times \text{altitude [km]}) \times (1 + (y - 250)/500)$ mm yr$^{-1}$ |
| Lake evaporation | 1300 mm yr$^{-1}$ |

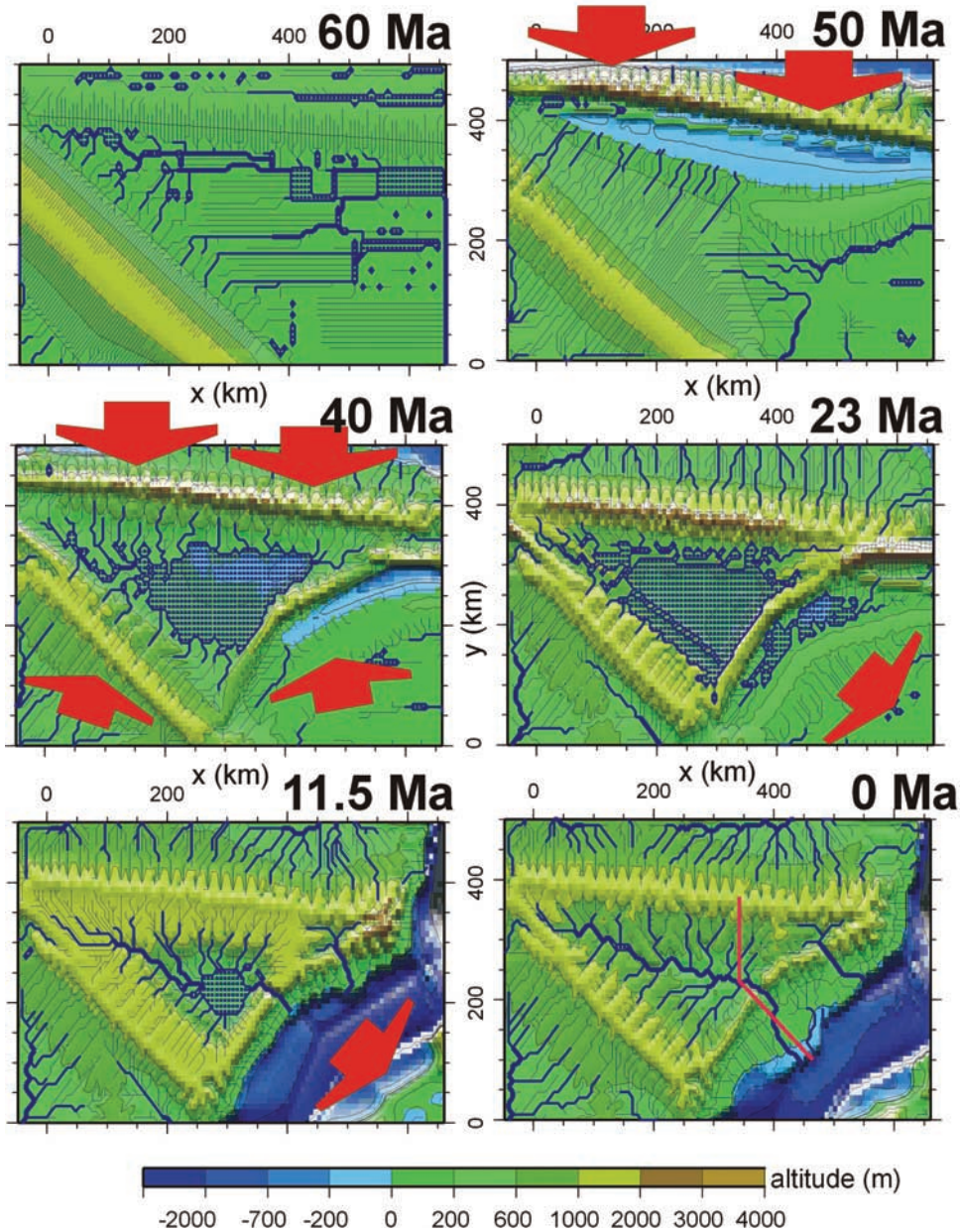


**Figure 10.** Topography and drainage predicted by the model for different time slices. At 60 Ma, the initial topography is adopted for the model. At 50 Ma, the earlier E-W oriented foreland basin becomes disconnected from the eastern boundary of the model. At 40 Ma, tectonic shortening along the Catalan Coastal Range, together with a high evaporation/precipitation ratio closes the drainage basin. At 23 Ma, extension in the Valencia Trough increases passive uplift of the Catalan Coastal Ranges. One of the streams in the new escarpment captures the endorheic drainage system, 11.5 Ma. Widespread incision affects the entire Ebro sedimentary basin, 0 Ma (present).

[54] Due to sediment accumulation in the postcompressional basin, the lake level increases from 150 m at 26 Ma to 1050 m at the time of lake capture. The capture or opening of the lake is predicted at 11.5 Ma, stimulating the formation of a strongly incising river network draining to the open sea and persisting to $t = 0$ (present). The process of lake capture itself (from the first contact of the lake with one of the east draining streams till the complete extinction of the lake) occurs in about 700 kyr. The age at which the model predicts the capture is sensitive to small variations in model parameters. For example, slight differences (beyond what is geologically constrainable) in the geometry of the tectonic blocks can favor the organization of drainage and/or reduce the width of the topographic barrier, speeding up the capture in several million years. Similarly, small changes on the paleoprecipitation and the paleoevaporation rates significantly change the time of opening, as seen in the previous subsection. Minor changes to the initial conditions of the model modify the particular location of every river, revealing this nonlinear, unpredictable character of drainage evolution. The overall

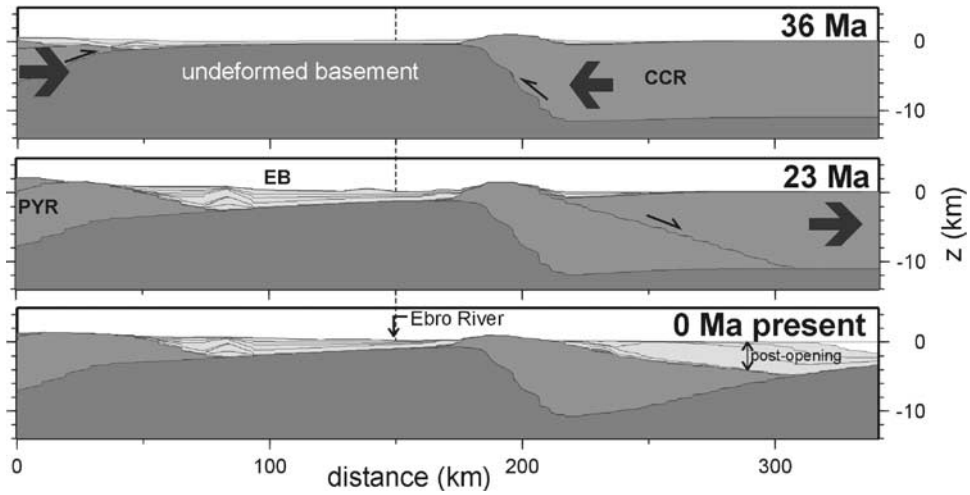


**Figure 11.** Cross sections corresponding to three stages of the model at 36 Ma (phase of tectonic convergence), 23 Ma (transition from convergence to extension), and 0 Ma (present). Extension in the Valencia Trough reduces the width of the Catalan Coastal Range. Sediment horizons correspond to 48, 45, 37, 33.5, 28.5, 23.5, 16.5, 11, 5.5, 2 Ma and present. Location of the cross section in Figure 10.

characteristics of the drainage pattern are most commonly related to the control exerted by the tectonic deformation [e.g., *Kühni and Pfiffner*, 2001]. However, in the case of the Ebro Basin, the nonlinear behavior exerts a first-order control because the lake capture, a dramatic change in drainage evolution, occurs in the posttectonic stage.

[55] Another feature reproduced in the model is the drainage change of the easternmost corner of the southern flank of the Pyrenees, from southwestward (basinward) to eastward (toward the Mediterranean). This change is a result of piracy undertaken by the new Mediterranean rivers on the NE corner of the former centripetal drainage of the closed basin, and it is in agreement with the development of the Ter and Llobregat Rivers [*Lewis et al.*, 2000] (Figure 1). Thus the model suggests that the distal location of these rivers with respect to the lakeshore impeded them to complete the lake capture.

[56] The predicted erosion-sedimentation budget undergoes three clear stages (Figure 12c). During the syncompression phase (before 25 Ma), the intramountain closed basin (corresponding to the Ebro Basin) is filled in at increasing rates as the topography and erosion in the surrounding ranges raise. The decrease in sediment accumulation rates at the end of this stage is related to the escape of part of the sediments to the open sea during transient lake overflows. During the postshortening endorheic phase (25–11.5 Ma), deposition in the basin continues with decreasing rates, whereas deposition in the small flexural basin SE of the Catalan Coastal Range occurs at low rates. The volume of sediments at the end of the closed stage (140,000 $km^3$) approximates the values calculated in the previous section. The model predicts that about 50% of that volume was deposited after the closure of the basin at 35 Ma, and only 15% (20,000 $km^3$) was deposited in the postcompression stage (after 25 Ma). Finally, during the posttectonic open phase (after 11.5 Ma), the basin and the tributary parts of the surrounding ranges undergo major river incision in which erosion products are transported to the open sea (corresponding to the Mediterranean). The final amount of sediment in the model basin is 102,000 $km^3$, close to the 111,000 $km^3$ obtained in the data compilation undertaken above. An amount of 85,300 $km^3$ is deposited during Neogene times in the Mediterranean, again in reasonable agreement with the 90,000 $km^3$ derived from the compilation by *Torné et al.* [1996].

[57] The total erosion rate occurring in the whole model domain (Figure 12c) increases during the compressive phase from 1200 $km^3$/Myr mostly in the SW passive border of the foreland basin (corresponding to the Iberian Range) to nearly 6000 $km^3$/Myr at 25 Ma (mostly in the Pyrenees). The exponential decrease to 2000 $km^3$/Myr after 25 Ma is only perturbed by the increased erosion due to the flank uplift in the eastern range (corresponding to the Catalan Coastal Range), mainly between 24 and 18 Ma. The postcompression erosion rate predicted in this model for the Pyrenees has maximum values of 45–60 m/Myr. The peaks in erosion and sedimentation rates in Figure 12c are related to the discrete movement of the thrusting units (the minimum amount of horizontal shift is one node). The same technical limitation explains that despite shortening along the Catalan Coastal Range is defined to start at 56 Ma (Table 2), the generation of topography along the corresponding fault starts only shortly after 50 Ma (Figure 10). To address the effects of numerical discretization on the predictions, we have carried out a number of simulations with double resolution, obtaining similar drainage evolutions. Although this can change the timing of drainage closure and opening by a few million years, the rates of basin infill and later basin incision are reasonably stable (changes induced by a double resolution amount less than 10%) due to the calibration of the transport model with the present-day rates of sediment delivery. Because of its high computation cost, we do not use this high resolution for the forward modeling undertaken in this paper.

[58] The main trends of the present topography are reproduced in the last stage of the model (Figure 10), such as the Ebro depression relative to the surrounding mountain chains and the Valencia Trough and the incision of the drainage network in the basin. The increase of topography in the

Pyrenees from west to east is not reproduced because we do not account for lateral variations of shortening along the orogen. The rate of fluvial sediment transport and the total sediment thickness at the final stage are shown in Figure 13.

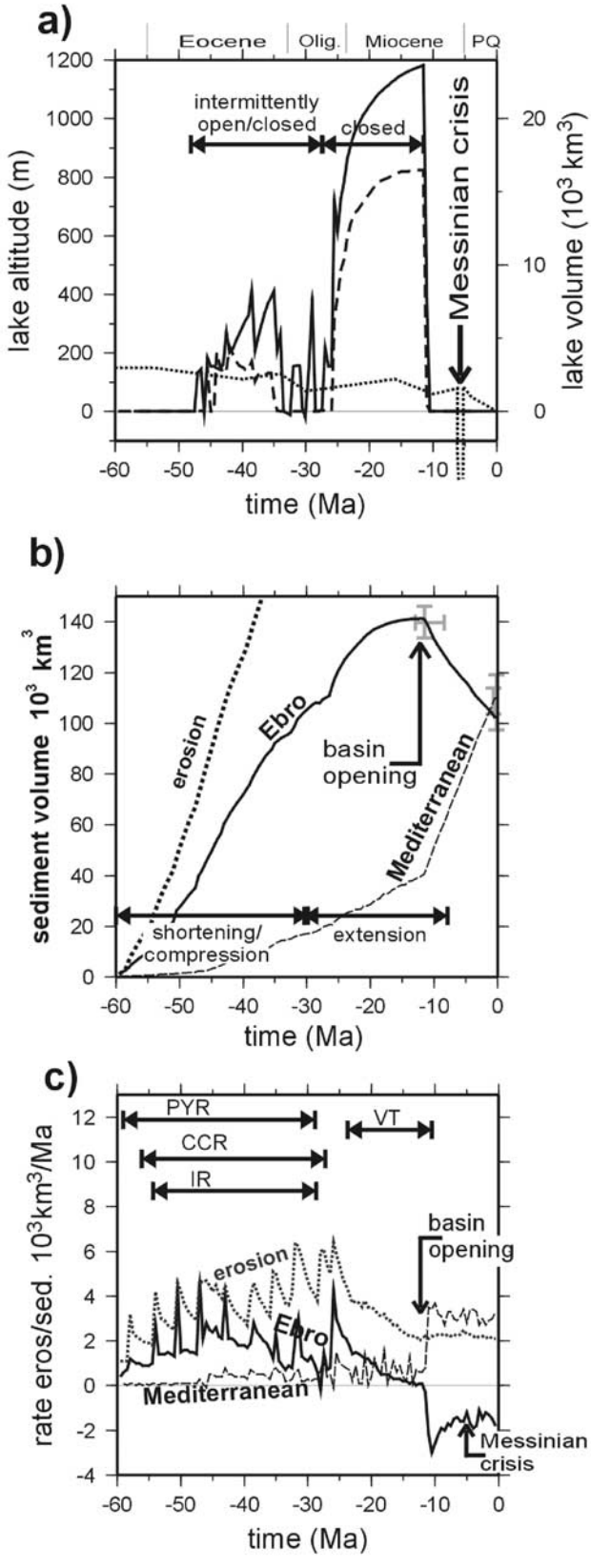


[59] The surface of the hydrographical basin corresponding to the Ebro in the final stage of the model is 89,600 km$^2$ and its mean water discharge is 1020 m$^3$/s, which is lower than historically observed (1530 m$^3$/s). This difference reflects the need for low precipitation rates (low $R$ and $K_R$ in equation (3)) to avoid an earlier drainage opening in the model.

## 5. Discussion

[60] Our models demonstrate the importance of the interplay between climatic, fluvial, and tectonic processes in shaping long-term landscape evolution and mass transport from mountain ranges to sedimentary basins. Most coupled tectonic-landscape evolution models have disregarded the role of lakes and their climate-controlled hydrographic balance (e.g., their endorheic/closed or exorheic/open character) in the evolution of continental topography and surface sediment transport, a feature of central importance in the present paper. From the present study, it appears that the presence of a closed Oligocene-Miocene lake in the Ebro Basin had a conspicuous influence on the landscape evolution and sediment budget of the south Pyrenean area.

### 5.1. Endorheic Period: Interplay Between Tectonics and Climate

[61] The models presented in this paper show that the drainage closure of the Ebro Basin transformed the basin into a trap for the debris from the surrounding mountain ranges, increasing the deposition rates and giving the Ebro Basin its singular architecture. The models also provide a validation of the hypothesis formulated by *Coney et al.* [1996] that thick accumulations of syntectnic and posttectonic conglomerates buried the frontal, presently outcropping Pyrenean thrusts at that stage. Vitrinite reflectance studies in the eastern Ebro Basin also suggest burial depths of the presently outcropping sediments varying between 2750 ± 250 m near the Pyrenean front and 950 ± 150 m near the Catalan Coastal Range [*Clavell*, 1992; *Waltham et al.*, 2000]. The model predictions above agree with these observations indicating that the removed sediment cover was up to 1500 m thick and provide an estimation of the maximum basin infill reached before the drainage opening of about 140,000 km$^3$.

[62] The models explain the existence of a single main lake body with a very asymmetric sediment distribution,

**Figure 12.** (opposite) (a) Predicted evolution for lake volume (dashed line) and water level (solid line) and adopted sea level changes (dotted line). Lake volume and lake level increase rapidly once the Ebro Basin becomes irreversibly endorheic (30 Ma in the model). (b) Predicted sediment volume through time for the model area corresponding to the Ebro Basin (bold line, maximum at the time of lake capture) and the Valencia Trough (dashed line). The dotted line indicates the accumulated eroded volume of mother rock over the entire model. (c) Erosion and sedimentation rates. Peaks are related to the discrete steps of crustal deformation. Note the increasing erosion rates during shortening in the three mountain ranges and the neglectable influence exerted by the sea level fall during the Messinian. Arrows indicate periods of tectonic deformation.

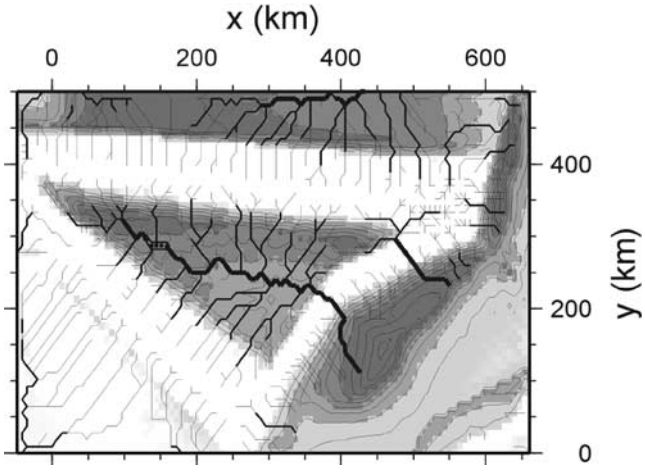


**Figure 13.** Predicted accumulated sediment thickness at $t = 0$ Ma (present) of the model shown in Figure 10. Isopachs are every 500 m. The predicted river network is drawn with line width proportional to sediment transport rate. Only those rivers transporting more than 0.3 kg/s are displayed.

both in facies and supply, as inferred by geological field studies [*Arenas and Pardo*, 1999]. The results presented above provide a quantitative framework for the understanding of these asymmetries as a result of the different tectonic evolution of the surrounding mountain ranges: The greater tectonic shortening and catchment areas in the Pyrenees and the Iberian Chain relative to the Catalan Coastal Range are shown to have produced and increased sediment supply from the north and southwest of the basin, slowly shifting the lake and the depocenter toward the SE.

[63] Our model results suggest that the closed Ebro paleolake was maintained for about 25 Myr by a dry climate with high evaporation/low precipitation rates and the extensional uplift of the Catalan Coastal Range. In the numerical models above, we require the mean precipitation rate during Neogene to be about 60% of the mean historical record and a high evaporation rate of 1300 mm/yr. The evaporation rate used lies among the extreme values recorded in present large lakes such as the Titicaca Lake and the Dead Sea and is much higher than the present 800 mm/yr evaporation rate in Lake Banyoles (NE from the Ebro Basin). Different parameter combinations keeping a similar precipitation/evaporation ratio can also fit the model, though still indicating a dry climate situation.

[64] These results show that the warm and arid climate during early Oligocene (33.7–28.5 Ma) reported by *Cavagnetto and Anadón* [1996] facilitated the onset of a closed lacustrine period that lasted about 25 Myr. The transition to humid conditions during the late Miocene [*Sanz de Siria Catalan*, 1993] with a relative peak at 9.4 Ma [*Alonso-Zarza and Calvo*, 2000; *Calvo et al.*, 1993] induced a lake level rise that probably favored the drainage opening of the Ebro Basin. As derived from our experiments, a relative short phase of wetter conditions with a duration of few hundred thousands of years could increase the lake level and trigger outlet erosion and irreversible basin opening. Due to the limited resolution of discretization in our models (related in turn to calculation time efficiency) it is not possible at the moment to further constrain these time lags required for capture irreversibility.

### 5.2. Opening and Incision of the Ebro Basin

[65] The opening of the Ebro endorheic drainage was previously interpreted as the result of escarpment erosion after extension along the Valencia Trough [*Riba et al.*, 1983]. According to this hypothesis, *Coney et al.* [1996] proposed that the sea level drop during the Messinian may have accelerated the basin opening by lowering the base level of the Mediterranean streams. However, the parameterization of lake capture shown in Figure 8 indicates that the Messinian base level lowering could not have a first-order impact on the timing of these events because its duration was too short. Drainage networks display a time lag after a base level pulse to reach the maximum incision efficiency [*Kooi and Beaumont*, 1996] and a drainage opening significantly later than Messinian would not account for the rework of sediment observed in the Ebro Basin.

[66] At least 22% (30,000 km$^3$) of the maximum detritic infill of the Ebro Basin was eroded and transported to the Mediterranean after the opening of the endorheic drainage. Including the additional material eroded from the Pyrenees and carried to the delta, the total postopening eroded mass in the Ebro catchment is at least $6.26 \times 10^{16}$ kg. Therefore the $4.8 \times 10^{16}$ kg of post-Messinian dry sediment in the delta reported by *Nelson* [1990] do not seem to account for the total deltaic accumulation, as frequently assumed in the literature [e.g., *Nelson and Maldonado*, 1990; *Coney et al.*, 1996].

[67] Our model predicts that in order to rework at least 30,000 km$^3$ of the Ebro Basin Tertiary infill, the opening of the drainage toward the Mediterranean should have occurred long before the Messinian, probably between 13 and 8.5 Ma (middle Serravallian to middle Tortonian). This result is supported by independent reports of large-scale pre-Messinian progradations [*Ziegler*, 1988; *Roca and Desegaulx*, 1992; *Roca*, 2001]. These siliciclastic progradations starting at middle Serravallian [Castellón Group, *Martínez del Olmo*, 1996] can be interpreted as related to the opening of the endorheic Ebro paleolake. The proposed age of opening would be also consistent with an important increase of the rate of sediment accumulation in the Valencia Trough [*Dañobeitia et al.*, 1990; *Martínez del Olmo*, 1996] and can be associated with a lake overflow during a coeval transition to wetter conditions [*Alonso-Zarza and Calvo*, 2000; *Sanz de Siria Catalan*, 1993].

[68] In addition to the classical concept of opening of the Ebro Basin by escarpment erosion driven by the Neogene Mediterranean streams, our modeling suggests that four additional large-scale processes played also a major role (Figure 6b): (1) partial tectonic (extensional) deconstruction of the topographic barrier (Catalan Coastal Range); (2) flexural flank uplift of the Catalan Coastal Range; (3) sediment overfill of the lake; and (4) lake level rise related to a long-term climatic change to wetter conditions.

[69] The development of the Valencia Trough had two opposite effects on the Ebro drainage. First, it facilitated the drainage opening by reducing the width of the topographic barrier of the Catalan Coastal Range and increasing the topographic gradient and erosion capacity of the short

streams developed in the new Mediterranean margin. Second, it delayed the opening by flexural uplift of the flanks of the Catalan Coastal Range [a process similar to that described by *Tucker and Slingerland*, 1994]. This uplift agrees with recent fission track data and isotope analyses by *Juez-Larré and Andriessen* [2002], indicating about 2500 m of Neogene exhumation above the present Paleozoic outcrops (~2000 m of rock uplift).

### 5.3. Interplay Between Lithospheric and Surface Processes

[70] The combination of well-dated episodes of basin evolution, long-term denudation rates, and sediment delivery rates together with numerical modeling provides a process-based approach to determine how tectonics and river dynamics shaped the present landscape of the NE part of the Iberian Peninsula.

[71] Foreland basins are generally regarded as sedimentary accumulations whose evolution depends mainly on the tectonic history of the adjacent orogen and the mechanical response of the foreland lithosphere. The study of the Ebro Basin carried out here demonstrates that the drainage history and the organization of the fluvial-lacustrine network are major additional factors controlling the basin evolution. The interaction between surface processes (climate, erosion, and transport) and lithospheric tectonic deformation [e.g., *Avouac and Burov*, 1996; *Willet*, 1999; *Beaumont et al.*, 2000; *Garcia-Castellanos*, 2002; *Cloetingh et al.*, 2002] appears to be the primary control on the termination of a ~25 Myr long period of endorheic drainage and sediment trapping in the Ebro Basin. Climate aridity, probably enhanced by the intramountain orographic situation, appears to prolong the sediment trapping and the closure of the basin. This feedback between aridity and basin closure appears to have been onset by the favorable tectonic setting.

[72] The interplay between lithospheric and surface processes is explicit in the models above in both directions: first, surface processes determine the way mass is redistributed in space and time, thus affecting the isostatic vertical movements. Second, the crustal and lithospheric-scale tectonics control and organize the nonlinear, chaotic nature of drainage networks. In the zones deformed by folding and thrusting, the long-term drainage evolution is controlled by the kinematics of tectonism [e.g., *Tucker and Slingerland*, 1996; *Kühni and Pfiffner*, 2001], but the second-order role of lithospheric flexure can also become relevant in undeformed areas such as the external margin of a foreland basin [*Burbank*, 1992; *Garcia-Castellanos*, 2002] or during the posttectonic erosional rebound of an escarpment [*Tucker and Slingerland*, 1994]. In the case of the Ebro Basin, the role of isostasy is enhanced because the timing of lake capture, a dramatic drainage change affecting a catchment of nearly 85,000 km$^2$, is very sensitive to the vertical movements of its eastern drainage divide.

## 6. Conclusions

[73] The present study provides a large-scale, quantitative perspective of the Cenozoic evolution of the Ebro Basin as a natural laboratory of interaction between tectonics, surface transport, and climate. The combination of computer simulation techniques linking lithospheric and surface processes, together with a compilation of geological and geophysical data and a large-scale sediment budget of the Pyrenees-Ebro Basin-Valencia Trough system, support the following conclusions:

[74] 1. The basic trends of the mass balance between the Ebro Basin, its surrounding cordilleras, and the Mediterranean Sea can be explained by the combined effect of tectonic crustal shortening and extension, lithospheric flexure, surface fluvial transport, and climatic controls.

[75] 2. The ~25 Myr endorheic period was characterized by a centripetal fluvial network draining to a single large central lake and was probably facilitated by climatic conditions dryer than at present.

[76] 3. Extension in the western Mediterranean produced two opposing effects on the topographic barrier limiting the Ebro Basin to the east: (1) topographic lowering and narrowing of the ancestral Catalan Coastal Range and development of new river system draining to the Mediterranean with increased erosion power and (2) the flexural uplift of the footwall of these extensional faults. The first effect favored the capture of the Ebro paleolake, whereas the second delayed it.

[77] 4. The opening of the Ebro Basin was a combined result of lake capture (piracy) caused by one of the new Mediterranean streams and sediment overfilling of the basin (probably facilitated by a short period of wetter climatic conditions during late Neogene). The sea level fall during the Messinian had a minor role in this drainage evolution.

[78] 5. The basin opening occurred most likely later than 13 Ma and earlier than 8.5 Ma. The large altitude difference between the Ebro paleolake and the Mediterranean Sea (~1000 m) and the large Ebro catchment area resulted in high incision rates at the time of the capture, making the drainage change irreversible after few hundred thousands years.

[79] **Acknowledgments.** We want to thank the stimulating discussions with C. Arenas, C. Taberner, H. Kooi, and J.A. Gil, who contributed to fine tune the models and the manuscript. The paper was substantially improved by constructive reviews from D. Burbank and J. Kuhlemann. M. Torné kindly provided the sediment thickness compilation for the Valencia Trough. This work has been funded by the Netherlands Center for Integrated Solid Earth Science (ISES).

## References

Aharon, P., S. L. Goldstein, C. W. Wheeler, and G. Jacobson, Sea-level events in the South Pacific linked with the Messinian salinity crisis, *Geology*, *21*, 771–775, 1993.

Alonso-Zarza, A. M., and J. P. Calvo, Palustrine sedimentation in an episodically subsiding basin: The Miocene of the northern Teruel Graben (Spain), *Palaeogeogr. Palaeoclimatol. Palaeoecol.*, *160*, 1–21, 2000.

Anadón, P., L. Cabrera, B. Colldeforns, and A. Sáez, Los sistemas lacustres del Eoceno superior y Oligoceno del sector oriental de la Cuenca del Ebro, *Acta Geol. Hispán.*, *24*, 205–230, 1989.

Arenas, C., and G. Pardo, Latest Oligocene-late Miocene lacustrine systems of the north-central part of the Ebro Basin (Spain): Sedimentary facies model and palaeogeographic synthesis, *Palaeogeogr. Palaeoclimatol. Palaeoecol.*, *151*, 127–148, 1999.

Arenas, C., J. Casanova, and G. Pardo, Stable-isotope characterization of the Miocene lacustrine systems of Los Monegros (Ebro Basin, Spain); palaeogeographic and palaeoclimatic implications, *Palaeogeogr. Palaeoclimatol. Palaeoecol.*, *128*, 133–155, 1997.

Arenas, C., H. Millán, G. Pardo, and A. Pocoví, Ebro Basin continental sedimentation associated with late compressional Pyrenean tectonics (north-eastern Iberia): Controls on basin margin fans and fluvial system, *Basin Res.*, *13*, 65–89, 2001.

Avouac, J. P., and E. B. Burov, Erosion as a driving mechanism of intracontinental mountain growth, *J. Geophys. Res.*, *101*, 17,747–17,769, 1996.

Bartrina, M. T., L. Cabrera, M. J. Jurado, J. Guimerá, and E. Roca, Evolution of the central Catalan margin of the Valencia Trough (western Mediterranean), *Tectonophysics*, *203*, 219–247, 1992.

Beaumont, C., Foreland basins, *Geophys. J. R. Astron. Soc.*, *65*, 291–329, 1981.

Beaumont, C., P. Fullsack, and J. Hamilton, Erosional control of active compressional orogens, in *Thrust Tectonics*, edited by K. R. McClay, pp. 1–18, Chapman and Hall, New York, 1992.

Beaumont, C., J. A. Muñoz, J. Hamilton, and P. Fullsack, Factors controlling the Alpine evolution of the central Pyrenees inferred from a comparison of observations and geodynamical models, *J. Geophys. Res.*, *105*, 8121–8145, 2000.

Burbank, D., Causes for recent uplift deduced from deposited patterns in the Ganges basin, *Nature*, *357*, 48–50, 1992.

Burbank, D. W., and J. Vergés, Reconstruction of topography and related depositional systems during active thrusting, *J. Geophys. Res.*, *99*, 20,281–20,297, 1994.

Burbank, D. W., C. Puigdefàbregas, and J. A. Muñoz, The chronology of the Eocene tectonic and stratigraphic development of the eastern Pyrenean foreland basin, northeast Spain, *Geol. Soc. Am. Bull.*, *104*, 1101–1120, 1992.

Cabrera, L., and A. Saez, Coal deposition in carbonate-rich shallow lacustrine systems: The Calaf and Mequinenza sequences (Oligocene, eastern Ebro basin, NE Spain), *J. Geol. Soc. London*, *144*, 451–4461, 1987.

Cabrera, L., M. Cabrera, R. Gorchs, and F. X. C. de las Heras, Lacustrine basin dynamics and organosulphur compound origin in a carbonate-rich lacustrine system (late Oligocene Mequinenza Formation, SE Ebro Basin, NE Spain), *Sediment. Geol.*, *148*, 289–317, 2002.

Calvo, J. P., et al., Up-to-date Spanish continental Neogene synthesis and paleoclimatic interpretation, *Rev. Soc. Geol. Esp.*, *6*, 29–40, 1993.

Cámara, P., and J. Klimowitz, Interpretación geodinámica de la vertiente centro-occidental surpirenaica (cuencas Jaca-Tremp), *Estud. Geol.*, *41*, 391–404, 1985.

Cavagnetto, C., and P. Anadón, Preliminary palynological data on floristic and climatic changes during the middle Eocene-early Oligocene of the eastern Ebro Basin, northeast Spain, *Rev. Palaeobot. Palynol.*, *92*(3–4), 281–305, 1996.

Choukroune, P., and ECORS Pyrenees Team, The ECORS Pyrenean deep seismic profile reflection data and the overall structure of an orogenic belt, *Tectonics*, *8*, 23–39, 1989.

Clavell, E., Geologia del petroli de les conques terciaries de Catalunya, Ph.D. thesis, Univ. of Barcelona, Barcelona, Spain, 1992.

Clavell, E., A. Martínez, and J. Vergés, Morfología del basament del Pirineu oriental: Evolucio I relacio amb mantells de corriment, *Acta Geol. Hispán.*, *23*(2), 129–140, 1988.

Cloetingh, S., E. Burov, F. Beekman, B. Andeweg, P. A. M. Andriessen, D. Garcia-Castellanos, G. de Vicente, and R. Vegas, Lithospheric folding in Iberia, *Tectonics*, *21*(5), 1041, doi::10.1029/2001TC901031, 2002.

Colomer, J., E. Roget, and X. Casamitjana, Daytime heat balance for estimating non-radiative fluxes of lake Banyoles, Spain, *Hydrol. Processes*, *10*, 721–726, 1996.

Coney, P. J., J. A. Muñoz, K. R. McKlay, and C. A. Evenchick, Syntectonic burial and post-tectonic exhumation of the Southern Pyrenees foreland fold-thrust belt, *J. Geol. Soc. London*, *153*, 9–16, 1996.

Dañobeitia, J., B. Alonso, and A. Maldonado, Geological framework of the Ebro continental margin and surrounding areas, *Mar. Geol.*, *95*, 265–287, 1990.

Fitzgerald, P. G., J. A. Muñoz, P. J. Coney, and S. L. Baldwin, Asymmetric exhumation across the Pyrenean orogen: Implications for the evolution of a collisional orogen, *Earth Planet. Sci. Lett.*, *173*, 157–170, 1999.

Flemings, P. B., and T. E. Jordan, A synthetic stratigraphic model of foreland basins development, *J. Geophys. Res.*, *94*, 3851–3866, 1989.

Ford, M., W. H. Lockorish, and N. J. Kusznir, Tertiary foreland sedimentation in the Southern Subalpine Chains, SE France: A geodynamic appraisal, *Basin Res.*, *11*, 315–336, 1999.

Garcia-Castellanos, D., Interplay between lithospheric flexure and river transport in foreland basins, *Basin Res.*, *14*, 89–104, 2002.

Garcia-Castellanos, D., M. Fernàndez, and M. Torne, Modeling the evolution of the Guadalquivir foreland basin (southern Spain), *Tectonics*, *21*(3), 1018, doi::10.1029/2001TC001339, 2002.

Gaspar-Escribano, J. M., J. D. Van Wees, M. Ter Voorde, S. Cloetingh, E. Roca, L. Cabrera, J. A. Muñoz, P. A. Ziegler, and D. Garcia-Castellanos, 3D flexural modeling of the Ebro Basin (NE Iberia), *Geophys. J. Int.*, *145*, 349–367, 2001.

Guimerà, J., and M. Álvaro, Structure et évolution de la compression alpine dans la Chaîne ibérique et la Chaîne côtière catalane (Espagne), *Bull. Soc. Geol. Fr.*, *6*, 339–348, 1990.

Haq, B. U., J. Hardenbol, and P. R. Vail, Chronology of fluctuating sea levels since the Triassic, *Science*, *235*, 1156–1167, 1987.

Howard, A. D., E. W. Dietrich, and A. M. Seidl, Modeling fluvial erosion on regional to continental scales, *J. Geophys. Res.*, *99*, 13,971–13,986, 1994.

Hsu, K. J., W. B. F. Ryan, and M. B. Cita, Late Miocene desiccation of the Mediterranean, *Nature*, *242*, 240–244, 1972.

Janssen, M. E., M. Torné, S. Cloetingh, and E. Banda, Pliocene uplift of the eastern Iberian margin; inferences from quantitative modelling of the Valencia Trough, *Earth Planet. Sci. Lett.*, *119*(4), 585–597, 1993.

Johnson, D. D., and C. Beaumont, Preliminary results from a planform kinematic model of orogen evolution, surface processes and the development of clastic foreland basin stratigraphy, in *Stratigraphic Evolution of Foreland Basins*, edited by S. L. Dorobek, and G. M. Ross, *SEPM Spec. Publ.*, *52*, 1–24, 1995.

Juez-Larré, J., and P. A. M. Andriessen, Post Late Paleozoic tectonism in the southern Catalan Coastal Ranges (NE Spain), assessed by apatite fission-track analysis, *Tectonophysics*, *349*, 367–368, 2002.

Jurado, M. J., and O. Riba, The Rioja Area (westernmost Ebro Basin): A ramp valley with neighbouring piggybacks, in *Tertiary Basins of Spain*, edited by P. F. Friend and C. Dabrio, pp. 173–179, Cambridge Univ. Press, New York, 1996.

Kooi, H., and C. Beaumont, Escarpment evolution on high-elevation rifted margins: Insights derived from a surface processes model that combines diffusion, advection, and reaction, *J. Geophys. Res.*, *99*, 12,191–12,209, 1994.

Kooi, H., and C. Beaumont, Large-scale geomorphology; classical concepts reconciled and integrated with contemporary ideas via a surface processes model, *J. Geophys. Res.*, *101*, 3361–3386, 1996.

Korzoun, V. I., A. A. Sokolov, and M. I. Budyko, *Atlas of the World Water Balance*, Hydrometeorol. Publ. House, St. Petersburg, Russia, 1977.

Krijgsman, W., F. J. Hilgen, I. Raffi, F. J. Sierro, and D. S. Wilson, Chronology, causes and progression of the Messinian salinity crisis, *Nature*, *400*, 652–655, 1999.

Kuhlemann, J., W. Frisch, I. Dunkl, and B. Szekely, Quantifying tectonic versus erosive denudation by the sediment budget: The Miocene core complexes of the Alps, *Tectonophysics*, *330*, 1–23, 2001.

Kühni, A., and O. A. Pfiffner, Drainage patterns and tectonic forcing: A model study for the Swiss Alps, *Basin Res.*, *13*, 169–197, 2001.

Lanaja, J. M., R. Querol, and A. Navarro, *Contribución de la Exploración Petrolífera al Conocimiento de la Geología de España*, 465 pp., Inst. Geol. y Min. de Esp., Madrid, Spain, 1987.

Lawton, T. F., E. Roca, and J. Guimerà, Kinematic-stratigarphic evolution of a growth syncline and its implications for tectonic development of the proximal foreland basin, southeastern Ebro Basin, Catalunya, Spain, *Geol. Soc. Am. Bull.*, *111*, 412–431, 1999.

Lewis, C. J., J. Vergés, and M. Marzo, High mountains in a zone of extended crust: Insights into the Neogene-Quaternary topographic development of northeastern Iberia, *Tectonics*, *19*, 86–102, 2000.

López-Blanco, M., M. Marzo, D. W. Burbank, J. Vergés, E. Roca, P. Anadón, and J. Piña, Tectonic and climatic controls on the development of foreland fan deltas: Montserrat and Sant Llorenç del Munt systems (middle Eocene, Ebro Basin, NE Spain), *Sediment. Geol.*, *138*, 17–39, 2000.

Martínez del Olmo, W., Depositional sequences in the Gulf of Valencia Tertiary Basin, in *Tertiary Basins of Spain the Stratigraphic Record of Crustal Kinematics: World and Regional Geology*, edited by P. F. Friend and C. J. Dabrio, pp. 55–67, Cambridge Univ. Press, New York, 1996.

Mauffret, A., G. Pascal, A. Maillard, and C. Gorini, Tectonics and deep structure of the north-western Mediterranean Basin, *Mar. Pet. Geol.*, *12*, 645–666, 1995.

Meigs, A. J., J. Vergés, and D. W. Burbank, Ten-million-year history of a thrust sheet, *Geol. Soc. Am. Bull.*, *108*, 1608–1625, 1996.

Muñoz, J. A., Evolution of a continental collision belt: ECORS-Pyrenees crustal balanced section, in *Thrust Tectonics*, edited by K. R. McClay, pp. 235–246, Chapman and Hall, New York, 1992.

Muñoz-Jiménez, A., and A. M. Casas-Sainz, The Rioja Trough (N Spain): Tectonosedimentary evolution of a symmetric foreland basin, *Basin Res.*, *9*, 65–85, 1997.

Negredo, A. M., M. Fernàndez, M. Torné, and C. Doglioni, Numerical modeling of simultaneous extension and compression; the Valencia Trough (western Mediterranean), *Tectonics*, *18*, 361–374, 1999.

Nelson, C. H., Estimated post-Messinian sediment supply and sedimentation rates on the Ebro continental margin, Spain, *Mar. Geol.*, *95*, 395–418, 1990.

Nelson, C. H., and A. Maldonado, Factors controlling late Cenozoic continental margin growth from the Ebro Delta to the western Mediterranean deep sea, *Mar. Geol.*, *95*, 419–440, 1990.

Pérez, A., A. Muñoz, G. Pardo, J. Villena, and C. Arenas, Las unidades tectosedimentarias del Neo'geno del Borde Ibérico de la Depresión del Ebro (sector central), in *Sistemas Lacustres Neógenos del Margen Ibérico de la Cuenca del Ebro*, edited by A. Pérez, A. Muñoz, and J. A. Sánchez, pp. 7–20, Secr. Publ. Univ. Zaragoza, Barcelona, Spain, 1988.

Pérez, A., A. Muñoz, G. Pardo, and J. Villena, Lacustrine Neogene deposits of the Ebro Basin (southern margin), northeastern Spain, in *Global Geological Record of Lake Basins*, edited by E. Gierslowski-Kordesch and K. Kelts, pp. 325–330, Cambridge Univ. Press, New York, 1994.

Pérez-Rivarés, F. J., M. Garcés, C. Arenas, and G. Pardo, Magnetocronología de la sucesión Miocena de la Sierra de Alcubierre (sector central de la cuenca del Ebro), *Rev. Soc. Geol. Esp.*, *15*(3–4), 211–225, 2002.

Puigdefàbregas, C., J. A. Muñoz, and J. Vergés, Thrusting and foreland basin evolution in the Southern Pyrenees, in *Thrust Tectonics*, edited by K. R. McClay, pp. 247–254, Chapman and Hall, New York, 1992.

Riba, O., S. Reguant, and J. Villena, Ensayo de síntesis estratigráfica y evolutiva de la cuenca terciaria del Ebro, in *Libro Jubilar J.M. Ríos*, *Geol. Esp.*, vol. II, pp. 131–159, Inst. Geol. y Min. de Esp., Madrid, 1983.

Roca, E., The northwest Mediterranean Basin (Valencia Trough, Gulf of Lions and Liguro-Provencal basins): Structure and geodynamic evolution, in *Peri-Tethys Memoir 6: Peri-Tethyan Rift/Wrench Basins and Passive Margins*, edited by P. A. Ziegler et al., *Mem. Mus. Natl. Hist. Nat.*, *186*, 671–706, 2001.

Roca, E., and P. Desegaulx, Analysis of the geological evolution and vertical movements in the Valencia Trough (western Mediterranean), *Mar. Pet. Geol.*, *9*, 167–185, 1992.

Roca, E., and J. Guimerà, The Neogene structure of the eastern Iberian margin; structural constraints on the crustal evolution of the Valencia Trough (western Mediterranean), *Tectonophysics*, *203*, 203–218, 1992.

Roca, E., M. Sans, L. Cabrera, and M. Marzo, Oligocene to middle Miocene evolution of the central Catalan margin northwestern Mediterranean), *Tectonophysics*, *315*, 209–233, 1999.

Roure, F., P. Choukroune, X. Berastegui, J. A. Muñoz, A. Villien, P. Matheron, M. Bareyt, M. Seguret, P. Camara, and J. Deramond, ECORS deep seismic data and balanced cross sections; geometric constraints on the evolution of the Pyrenees, *Tectonics*, *8*, 41–50, 1989.

Salas, R., J. Guimerà, R. Mas, C. Martín-Closas, A. Meléndez, and A. Alonso, Evolution of the Mesozoic Central Iberian Rift system and its Cenozoic inversion (Iberian chain), in *Peri-Tethys Memoir 6: Pery-Tethyan Rift/Wrench Basins and Passive Margins*, edited by P. A. Ziegler et al., *Mem. Mus. Nat. d'Histore Nat.*, *186*, 145–185, 2001.

Sánchez, J. A., P. Coloma, and A. Pérez, Sedimentary processes related to the groundwater flows from the Mesozoic Carbonate Aquifer of the Iberian Chain in the Tertiary Ebro Basin, northeast Spain, *Sediment. Geol.*, *129*, 201–213, 1999.

Sanz de Siria Catalan, A., Datos sobre la paleoclimatologia y paleoecologia del Neogeno del Valles-Penedes segun las macrofloras halladas en la cuenca y zonas proximas, *Paleontol. Evol.*, *26–27*, 281–289, 1993.

Serra-Raventós, J., El sistema sedimentario del Delta del Ebro (The sedimentary system of the Ebro Delta), *Rev. Obras Publ. 3368*, pp. 15–22, Esc. de Ing. de Caminos, Madrid, Spain, 1997.

Serrat, D., La xarxa fluvial dels Països Catalans, in *Història Natural dels Països Catalans, v. Geologia II*, pp. 375–389, Enciclopedia Catalana, Barcelona, Spain, 1992.

Sinclair, H. D., and P. A. Allen, Vertical vs. horizontal motions in the Alpine orogenic wedge: Stratigraphic response in the foreland basin, *Basin Res.*, *4*, 215–232, 1992.

Sobel, E. R., G. E. Hilley, and M. R. Strecker, Formation of internally drained contractional basins by aridity-limited bedrock incision, *J. Geophys. Res.*, *108*, doi:10.1029/2002JB001883, in press, 2003.

Taberner, C., J. Dinarès-Turell, J. Giménez, and C. Docherty, Basin infill architecture and evolution from magnetostratigraphic cross-basin correlations in the southeastern Pyrenean foreland basin, *Geol. Soc. Am. Bull.*, *111*,1155–1174, 1999.

Teixell, A., The Ansó transect of the southern Pyrenees: Basement and cover thrust geometries, *J. Geol. Soc. London*, *153*, 301–310, 1996.

Teixell, A., Crustal structure and orogenic material budget in the west central Pyrenees, *Tectonics*, *17*, 395–406, 1998.

Torné, M., E. Banda, and M. Fernàndez, The Valencia Trough: Geological and geophysical constraints on basin formation models, in *Peri-Tethys Memoir 2: Structure and Prospects of Alpine Basins and Forelands*, edited by P. A. Ziegler and F. Horvath, *Mem. Mus. Natl. Hist. Nat.*, *170*, 103–128, 1996.

Tucker, G. E., and R. L. Slingerland, Erosional dynamics, flexural isostasy, and long-lived escarpments: A numerical modeling study, *J. Geophys. Res.*, *99*, 12,229–12,243, 1994.

Tucker, G. E., and R. L. Slingerland, Predicting sediment flux from fold and thrust belts, *Basin Res.*, *8*, 329–349, 1996.

Turner, J. P., Switches in subduction direction and the lateral termination of mountain belts: Pyrenees-Cantabrian transition, Spain, *J. Geol. Soc. London*, *153*, 563–571, 1996.

van der Beek, P., and J. Braun, Controls on post-Mid-Cretaceous landscape evolution in the southeastern highlands of Australia; insights from numerical surface process models, *J. Geophys. Res.*, *104*, 4945–4966, 1999.

van Wees, J. D., and S. Cloetingh, A finite-difference technique to incorporate spatial variations in rigidity and planar faults into 3-D models for lithospheric flexure, *Geophys. J. Int.*, *117*, 179–195, 1994.

Vergés, J., and F. Sàbat, Constraints on the western Mediterranean kinematics evolution along a 1,000-km transect from Iberia to Africa, in *The Mediterranean Basins: Tertiary Extension within the Alpine Orogen*, edited by B. Durand et al., *Geol. Soc. Spec. Publ.*, *156*, 63–80, 1999.

Vergés, J., H. Millán, E. Roca, J. A. Muñoz, M. Marzo, J. Cirés, T. den Bezemer, R. Zoetemeijer, and S. Cloetingh, Eastern Pyrenees and related foreland basins: Pre-, syn- and post-collisional crustal-scale cross-sections, *Mar. Pet. Geol.*, *12*, 903–915, 1995.

Vergés, J., M. Marzo, J. Santaeularia, J. Serra-Kiel, D. W. Burbank, J. A. Muñoz, and J. Giménez-Montsant, Quantified vertical motions and tectonic evolution of the SE Pyrenean foreland basin, in *Cenozoic Foreland Basins of Western Europe*, edited by A. Mascle et al., *Geol. Soc. Spec. Publ.*, *134*, 107–134, 1998.

Vörösmarty, C. J., B. Fekete, and B. A. Tucker, River discharge database, version 1.0 (RivDIS v1.0), A contribution to IHP-V theme 1. Technical documents in hydrology series, UNESCO, Paris, 1996. (Available at http://www.rivdis.sr.unh.edu/)

Waltham, D., C. Docherty, and C. Taberner, Decoupled flexure in the South Pyrenean foreland, *J. Geophys. Res.*, *105*, 16,329–16,340, 2000.

Watts, A. B., and M. Torné, Crustal structure and the mechanical properties of extended continental lithosphere in the Valencia Trough (western Mediterranean), *J. Geol. Soc. London*, *149*, 813–827, 1992a.

Watts, A. B., and M. Torné, Subsidence history, crustal structure, and thermal evolution of the Valencia Trough; a young extensional basin in the western Mediterranean, *J. Geophys. Res.*, *97*, 20,021–20,041, 1992b.

Whipple, K. X., and G. E. Tucker, Dynamics of the stream-power river incision model; implications for height limits of mountain ranges, landscape response timescales, and research needs, *J. Geophys. Res.*, *104*, 17,661–17,674, 1999.

Willet, S. D., Orogeny and orography: The effects of erosion on the structure of mountain belts, *J. Geophys. Res.*, *104*, 28,957–28,981, 1999.

Willgoose, G., R. L. Bras, and I. Rodriguez-Iturbe, A physically based coupled channel network growth and hillslope evolution model (3 sections), *Water Resour. Res.*, *27*, 1671–1702, 1991.

Ziegler, P. A., Evolution of the Artic-North Atlantic and the Western Tethys, *AAPG Mem., 43*, 198 pp., 1988.

---

S. Cloetingh, D. Garcia-Castellanos, and J. Gaspar-Escribano, Faculty of Earth Sciences, Vrije Universiteit, De Boelelaan, 1085, 1081HV Amsterdam, Netherlands. (gard@geo.vu.nl)

J. Vergés, Institute of Earth Sciences "Jaume Almera" (CSIC), Solé i Sabarís s/n, 08028 Barcelona, Spain.